The measurement of α_s from event shapes with the DELPHI detector at the highest LEP energies

Abdallah (et al.), J.; Blom, H.M.; Kluit, P.M.; Ferreira-Montenegro, J.; Mulders, M.P.; Reid, D.W.; Timmermans, J.J.M.; van Dam, P.H.A.

Link to publication

The measurement of α_s from event shapes with the DELPHI detector at the highest LEP energies

DELPHI Collaboration

J. Abdallah[25], P. Abreu[22], W. Adam[51], P. Adzic[11], T. Albrecht[17], T. Alderweireld[2], R. Alemany-Fernandez[8], T. Allmendinger[17], P. Allport[23], U. Amaldi[29], N. Amapane[45], S. Amato[48], E. Anashkin[36], A. Andreazza[28], S. Andringa[22], N. Anjos[22], P. Antilogus[25], W-D. Apel[17], Y. Arnoud[14], S. Ask[26], B. Asman[44], E. Augustin[25], A. Augustinus[8], P. Baillon[8], A. Ballestrero[46], P. Bambade[20], R. Barbier[27], D. Bardin[16], J. Barker[17], A. Baroncelli[39], M. Battaglia[8], M. Baubillier[25], K-H. Becks[53], M. Begalli[6], A. Behrmann[53], E. Ben-Haim[20], N. Benekos[32], A. Benvenuti[5], C. Berat[14], M. Berggren[25], L. Berntzon[44], D. Bertrand[2], M. Besancon[40], N. Besson[40], D. Bloch[9], M. Blom[31], M. Bluj[52], M. Bonesini[29], M. Boonekamp[40], L. Booth[23], G. Borisov[21], O. Botner[49], B. Bouquet[20], V. Bowcock[23], I. Boyko[16], M. Bracko[43], R. Brenner[49], E. Brodet[35], P. Bruckman[18], M. Brunet[7], L. Bugge[33], P. Buschmann[53], M. Calvi[29], T. Camporesi[8], V. Canale[38], F. Carena[8], N. Castro[22], F. Cavallo[5], M. Chapkin[42], Ph. Charpentier[8], P. Checchia[36], R. Chierici[8], P. Chliapnikov[42], J. Chudoba[8], U. Chung[8], K. Cieslik[18], P. Collins[8], R. Contri[13], G. Cosme[20], F. Cossutti[47], J. Costa[50], D. Crennell[37], J. Cuevas[34], J. D'Hondt[2], J. Dalmau[44], T. da Silva[48], W. Da Silva[25], G. Della Ricca[47], A. De Angelis[47], W. De Boer[17], C. De Clercq[2], B. De Lotto[47], N. De Maria[45], A. De Min[36], L. de Paula[48], L. Di Ciaccio[38], A. Di Simone[39], K. Doroba[52], J. Drees[53,8], M. Dris[32], G. Eigen[4], T. Ekelof[49], M. Ellert[49], M. Elsing[8], C. Espirito Santo[22], G. Fanourakis[11], D. Fassouliotis[11,3], M. Feindt[17], J. Fernandez[41], A. Ferrer[50], F. Ferro[13], U. Flagmeyer[53], H. Foeth[8], E. Fokitis[32], F. Fulda-Quenzer[20], J. Fuster[50], M. Gandelman[48], C. Garcia[50], Ph. Gavillet[8], E. Gazis[32], R. Gokieli[8,52], B. Golob[43], G. Gomez-Ceballos[41], P. Goncalves[22], E. Graziani[39], G. Grosdidier[20], K. Grzelak[52], J. Guy[37], C. Haag[17], A. Hallgren[49], K. Hamacher[53], K. Hamilton[35], S. Haug[33], F. Hauler[17], V. Hedberg[26], M. Hennecke[17], H. Herr[8], J. Hoffman[52], S-O. Holmgren[44], J. Holt[8], A. Houlden[23], K. Hultqvist[44], N. Jackson[23], G. Jarlskog[26], P. Jarry[40], D. Jeans[35], K. Johansson[44], D. Johansson[44], P. Jonsson[27], C. Joram[8], L. Jungermann[17], F. Kapusta[25], S. Katsanevas[27], E. Katsoufis[32], G. Kernel[43], P. Kersevan[8,43], U. Kerzel[17], A. Kiiskinen[15], T. King[23], J. Kjaer[8], P. Kluit[31], P. Kokkinias[11], C. Kourkoumelis[3], O. Kouznetsov[16], Z. Krumstein[16], M. Kucharczyk[18], J. Lamsa[1], G. Leder[51], F. Ledroit[14], L. Leinonen[44], R. Leitner[30], J. Lemonne[2], V. Lepeltier[20], T. Lesiak[18], W. Liebig[53], D. Liko[51], A. Lipniacka[44], H. Lopes[48], M. Lopez[34], D. Loukas[11], P. Lutz[40], L. Lyons[35], J. MacNaughton[51], A. Malek[53], S. Maltezos[32], F. Mandl[51], J. Marco[41], R. Marco[41], B. Marechal[48], M. Margoni[36], J-C. Marin[8], C. Mariotti[8], A. Markou[11], C. Martinez-Rivero[41], J. Masik[12], N. Mastroyiannopoulos[11], F. Matorras[41], C. Matteuzzi[29], F. Mazzucato[36], M. Mazzucato[36], R. Mc Nulty[23], C. Meroni[28], E. Migliore[45], W. Mitaroff[51], U. Mjoernmark[26], T. Moa[44], M. Moch[17], K. Moenig[8,10], R. Monge[13], J. Montenegro[31], D. Moraes[48], S. Moreno[22], P. Morettini[13], U. Mueller[53], K. Muenich[53], M. Mulders[31], L. Mundim[6], W. Murray[37], B. Muryn[19], G. Myatt[35], T. Myklebust[33], M. Nassiakou[11], F. Navarria[5], K. Nawrocki[52], R. Nicolaidou[40], M. Nikolenko[16,9], A. Oblakowska-Mucha[19], V. Obraztsov[42], A. Olshevski[16], A. Onofre[22], R. Orava[15], K. Osterberg[15], A. Ouraou[40], A. Oyanguren[50], M. Paganoni[29], S. Paiano[5], P. Palacios[23], H. Palka[18], D. Papadopoulou[32], L. Pape[8], C. Parkes[24], F. Parodi[13], U. Parzefall[8], A. Passeri[39], O. Passon[53], L. Peralta[22], V. Perepelitsa[50], A. Perrotta[5], A. Petrolini[13], J. Piedra[41], L. Pieri[39], F. Pierre[40], M. Pimenta[22], E. Piotto[8], T. Podobnik[43], V. Poireau[8], E. Pol[6], G. Polok[18], V. Pozdniakov[16], N. Pukhaeva[2,16], A. Pullia[29], J. Rames[12], A. Read[33], P. Rebecchi[8], J. Rehn[17], D. Reid[31], R. Reinhardt[53], P. Renton[35], F. Richard[20], J. Ridky[12], M. Rivero[41], D. Rodriguez[41], A. Romero[45], P. Ronchese[36], P. Roudeau[20], T. Rovelli[5], V. Ruhlmann-Kleider[40], D. Ryabtchikov[42], A. Sadovsky[16], L. Salmi[15], J. Salt[50], C. Sander[17], A. Savoy-Navarro[25], U. Schwickerath[8], A. Segar[35], R. Sekulin[37], M. Siebel[53], A. Sisakian[16], G. Smadja[27], O. Smirnova[26], A. Sokolov[42], A. Sopczak[21], R. Sosnowski[52], T. Spassov[8], M. Stanitzki[17], A. Stocchi[20], J. Strauss[51], B. Stugu[4], M. Szczekowski[52], M. Szeptycka[52], T. Szumlak[19], T. Tabarelli[29], C. Taffard[23], F. Tegenfeldt[49], J. Timmermans[31], L. Tkatchev[16], M. Tobin[23], S. Todorovova[12], B. Tome[22], A. Tonazzo[29], P. Tortosa[50], P. Travnicek[12], D. Treille[8], G. Tristram[7], M. Trochimczuk[52], C. Troncon[28], M-L. Turluer[40], A. Tyapkin[16], P. Tyapkin[16], S. Tzamarias[11], V. Uvarov[42], G. Valenti[5], P. Van Dam[31], J. Van Eldik[8], A. Van Lysebetten[2], N. van Remortel[2], I. Van Vulpen[8], G. Vegni[28], F. Veloso[22], W. Venus[37], P. Verdier[27], V. Verzi[38], D. Vilanova[40], L. Vitale[47], V. Vrba[12], H. Wahlen[53], J. Washbrook[23], C. Weiser[17], D. Wicke[8], J. Wickens[2], G. Wilkinson[35], M. Winter[9], M. Witek[18], O. Yushchenko[42], A. Zalewska[18], P. Zalewski[52], D. Zavrtanik[43], V. Zhuravlov[16], I. Zimin[16], A. Zintchenko[16], M. Zupan[11]

[1] Department of Physics and Astronomy, Iowa State University, Ames IA 50011-3160, USA

[2] Physics Department, Universiteit Antwerpen, Universiteitsplein 1, 2610 Antwerpen, Belgium
and IIHE, ULB-VUB, Pleinlaan 2, 1050 Brussels, Belgium
and Faculté des Sciences, Univ. de l'Etat Mons, Av. Maistriau 19, 7000 Mons, Belgium

[3] Physics Laboratory, University of Athens, Solonos Str. 104, 10680 Athens, Greece

[4] Department of Physics, University of Bergen, Allégaten 55, 5007 Bergen, Norway

[5] Dipartimento di Fisica, Università di Bologna and INFN, Via Irnerio 46, 40126 Bologna, Italy

[6] Centro Brasileiro de Pesquisas Físicas, rua Xavier Sigaud 150, 22290 Rio de Janeiro, Brazil
and Depto. de Física, Pont. Univ. Católica, C.P. 38071 22453 Rio de Janeiro, Brazil
and Inst. de Física, Univ. Estadual do Rio de Janeiro, rua São Francisco Xavier 524, Rio de Janeiro, Brazil

[7] Collège de France, Lab. de Physique Corpusculaire, IN2P3-CNRS, 75231 Paris Cedex 05, France

[8] CERN, 1211 Geneva 23, Switzerland

[9] Institut de Recherches Subatomiques, IN2P3 - CNRS/ULP - BP20, 67037 Strasbourg Cedex, France

[10] Now at DESY-Zeuthen, Platanenallee 6, 15735 Zeuthen, Germany

[11] Institute of Nuclear Physics, N.C.S.R. Demokritos, P.O. Box 60228, 15310 Athens, Greece

[12] FZU, Inst. of Phys. of the C.A.S. High Energy Physics Division, Na Slovance 2, 180 40, Praha 8, Czech Republic

[13] Dipartimento di Fisica, Università di Genova and INFN, Via Dodecaneso 33, 16146 Genova, Italy

[14] Institut des Sciences Nucléaires, IN2P3-CNRS, Université de Grenoble 1, 38026 Grenoble Cedex, France

[15] Helsinki Institute of Physics, P.O. Box 64, 00014 University of Helsinki, Finland

[16] Joint Institute for Nuclear Research, Dubna, Head Post Office, P.O. Box 79, 101 000 Moscow, Russian Federation

[17] Institut für Experimentelle Kernphysik, Universität Karlsruhe, Postfach 6980, 76128 Karlsruhe, Germany

[18] Institute of Nuclear Physics PAN, Ul. Radzikowskiego 152, 31142 Krakow, Poland

[19] Faculty of Physics and Nuclear Techniques, University of Mining and Metallurgy, 30055 Krakow, Poland

[20] Université de Paris-Sud, Lab. de l'Accélérateur Linéaire, IN2P3-CNRS, Bât. 200, 91405 Orsay Cedex, France

[21] School of Physics and Chemistry, University of Lancaster, Lancaster LA1 4YB, UK

[22] LIP, IST, FCUL - Av. Elias Garcia, 14-1°, 1000 Lisboa Codex, Portugal

[23] Department of Physics, University of Liverpool, P.O. Box 147, Liverpool L69 3BX, UK

[24] Dept. of Physics and Astronomy, Kelvin Building, University of Glasgow, Glasgow G12 8QQ

[25] LPNHE, IN2P3-CNRS, Univ. Paris VI et VII, Tour 33 (RdC), 4 place Jussieu, 75252 Paris Cedex 05, France

[26] Department of Physics, University of Lund, Sölvegatan 14, 223 63 Lund, Sweden

[27] Université Claude Bernard de Lyon, IPNL, IN2P3-CNRS, 69622 Villeurbanne Cedex, France

[28] Dipartimento di Fisica, Università di Milano and INFN-MILANO, Via Celoria 16, 20133 Milan, Italy

[29] Dipartimento di Fisica, Univ. di Milano-Bicocca and INFN-MILANO, Piazza della Scienza 2, 20126 Milan, Italy

[30] IPNP of MFF, Charles Univ., Areal MFF, V Holesovickach 2, 180 00, Praha 8, Czech Republic

[31] NIKHEF, Postbus 41882, 1009 DB Amsterdam, The Netherlands

[32] National Technical University, Physics Department, Zografou Campus, 15773 Athens, Greece

[33] Physics Department, University of Oslo, Blindern, 0316 Oslo, Norway

[34] Dpto. Fisica, Univ. Oviedo, Avda. Calvo Sotelo s/n, 33007 Oviedo, Spain

[35] Department of Physics, University of Oxford, Keble Road, Oxford OX1 3RH, UK

[36] Dipartimento di Fisica, Università di Padova and INFN, Via Marzolo 8, 35131 Padua, Italy

[37] Rutherford Appleton Laboratory, Chilton, Didcot OX11 OQX, UK

[38] Dipartimento di Fisica, Università di Roma II and INFN, Tor Vergata, 00173 Rome, Italy

[39] Dipartimento di Fisica, Università di Roma III and INFN, Via della Vasca Navale 84, 00146 Rome, Italy

[40] DAPNIA/Service de Physique des Particules, CEA-Saclay, 91191 Gif-sur-Yvette Cedex, France

[41] Instituto de Fisica de Cantabria (CSIC-UC), Avda. los Castros s/n, 39006 Santander, Spain

[42] Inst. for High Energy Physics, Serpukov P.O. Box 35, Protvino, (Moscow Region), Russian Federation

[43] J. Stefan Institute, Jamova 39, 1000 Ljubljana, Slovenia and Laboratory for Astroparticle Physics, Nova Gorica Polytechnic,
Kostanjeviska 16a, 5000 Nova Gorica, Slovenia,
and Department of Physics, University of Ljubljana, 1000 Ljubljana, Slovenia

[44] Fysikum, Stockholm University, Box 6730, 113 85 Stockholm, Sweden

[45] Dipartimento di Fisica Sperimentale, Università di Torino and INFN, Via P. Giuria 1, 10125 Turin, Italy

[46] INFN, Sezione di Torino, and Dipartimento di Fisica Teorica, Università di Torino, Via P. Giuria 1, 10125 Turin, Italy

[47] Dipartimento di Fisica, Università di Trieste and INFN, Via A. Valerio 2, 34127 Trieste, Italy
and Istituto di Fisica, Università di Udine, 33100 Udine, Italy

[48] Univ. Federal do Rio de Janeiro, C.P. 68528 Cidade Univ., Ilha do Fundão 21945-970 Rio de Janeiro, Brazil

[49] Department of Radiation Sciences, University of Uppsala, P.O. Box 535, 751 21 Uppsala, Sweden

[50] IFIC, Valencia-CSIC, and D.F.A.M.N., U. de Valencia, Avda. Dr. Moliner 50, 46100 Burjassot (Valencia), Spain

[51] Institut für Hochenergiephysik, Österr. Akad. d. Wissensch., Nikolsdorfergasse 18, 1050 Vienna, Austria

[52] Inst. Nuclear Studies and University of Warsaw, Ul. Hoza 69, 00681 Warsaw, Poland

[53] Fachbereich Physik, University of Wuppertal, Postfach 100 127, 42097 Wuppertal, Germany

Abstract. Hadronic event shape distributions are determined from data in e^+e^- collisions between 183 and 207 GeV. From these the strong coupling α_s is extracted in $\mathcal{O}(\alpha_s^2)$, NLLA and matched $\mathcal{O}(\alpha_s^2)$+NLLA theory. Hadronisation corrections evaluated with fragmentation model generators as well as an analytical power ansatz are applied. Comparing these measurements to those obtained at and around M_Z allows a combined measurement of α_s from all DELPHI data and a test of the energy dependence of the strong coupling.

1 Introduction

Measurements of the strong coupling, α_s, of quantum chromodynamics [1] (QCD), the theory of strong interaction, using different observables and different analysis methods serve as an important consistency test of QCD. Once α_s is measured at a given scale, QCD predicts its energy dependence as described by the renormalisation group equation. A measurement of the strong coupling at different scales allows therefore a test of this important prediction, which is related to the property of asymptotic freedom [2].

At LEP, hadronic final states of the e^+e^- annihilation are used to study QCD. While the process $e^+e^- \to q\bar{q}$ is described by the electroweak theory alone, the radiation of gluons carries sensitivity to properties of the strong interaction. Our analysis uses event shape observables to measure the strong coupling. These dimensionless quantities characterize the topology of the events, e.g. whether the radiation of hard gluons gave rise to further jets.

The strong coupling is measured by comparing experimental cross-sections, $\frac{1}{\sigma}\frac{d\sigma}{dy}$, for an observable y with the theoretical predictions in which α_s enters as a free parameter. But since QCD is the theory of (asymptotically) free quarks and gluons, hadronisation effects need to be accounted for. This may be done either with phenomenological models [3–5], or with the help of QCD-inspired power corrections [6].

The QCD calculation can be performed in different ways as well. The earliest results were based on fixed-order perturbation theory [7]. For the observables studied here these predictions are limited to the three-jet region. An extension to the four-jet region would need next-to-next-to-leading-order (NNLO) corrections to be calculated. On the other hand the applicability of these calculations close to the two-jet region is limited as well, since in this kinematic domain enhanced logarithms occur [8]. To extend the applicability into the two-jet region the summation of these logarithms was developed, the so called next-to-leading-log approximation (NLLA) [8,9]. Finally the fixed-order results can be combined with NLLA calculations leading to the $\mathcal{O}(\alpha_s^2)$+NLLA matched theory for the cross-section, $R = \int \frac{1}{\sigma}\frac{d\sigma}{dy}dy$, [8,9]. According to different "matching schemes", these calculations are referred to as e.g. R or $\log R$ matching [8].

As a consequence of renormalisation, all perturbative QCD calculations to finite order depend upon the renormalisation scale μ, which is an unphysical parameter. The choice of μ is conventional and the effect of its variation is usually used to estimate the theoretical uncertainty. In the NLLA and matched theory even more arbitrary parameters enter, related to the phase-space boundary. We will discuss this point and our definition of the theoretical uncertainties in Sect. 4.1.

This paper presents the measurements of event shape distributions in e^+e^- collisions between 183 and 207 GeV. The data have been reprocessed in 2001 and our final results supersede some earlier DELPHI measurements at the corresponding energies [10]. Another change with respect to the previous LEP2 analysis is the use of improved event generators for both acceptance correction and background subtraction (see Sect. 2).

From the event shapes Thrust, C parameter, heavy jet mass, wide and total jet broadening, α_s is extracted with four different methods: the differential distributions are compared to predictions in $\mathcal{O}(\alpha_s^2)$, pure NLLA and $\mathcal{O}(\alpha_s^2)$+NLLA (logR), folded with fragmentation models, and in the fourth method the strong coupling is extracted from the mean values using an analytical power correction ansatz. An extension of this analysis with respect to the previous one [10] is the use of five observables instead of thrust and heavy jet mass only. Additionally the matching procedure for the $\mathcal{O}(\alpha_s^2)$+NLLA (logR) prediction has been modified. For consistency the distributions at M_Z from [10] have been refitted for these five observables (and with the same fit ranges). The combination of five α_s values for each method and energy makes the treatment of correlations more crucial. Section 4.2 is devoted to this topic.

From here the analysis proceeds in two steps: first the α_s values (together with the results from previous measurements at other LEP2 energies and LEP1 data) are used to test the QCD predicted scale dependence, i.e. to measure the β function of the strong interaction. Second, assuming the QCD β function, all α_s values at LEP1 and LEP2 are evolved to a reference energy and combined to a single α_s value for each method. It turns out that the weight of the LEP2 data in the combined α_s results is comparable to the weight of the LEP1 data alone. This unexpected result is due to the fact that at LEP2 the bigger statistical uncertainties are compensated for by smaller hadronisation and scale uncertainties.

The paper is organized as follows: in Sect. 2 the selection of hadronic events, the determination of the centre-of-mass energy, the correction procedures applied to the data, and the suppression of WW and ZZ events are briefly discussed. Section 3 presents event shapes and the comparison of the data with predictions from different generators. The measurements of α_s from differential distributions are discussed in Sect. 4, while Sect. 5 describes the α_s determination from mean values with power corrections. In Sect. 6 the running of the strong coupling is discussed and Sect. 7 contains

the combination of all α_s measurements. Section 8 gives a summary of the results.

2 Selection and correction of hadronic data

The analysis is based on data taken with the DELPHI detector in the years from 1997 to 2000 at centre-of-mass energies between 183 and 207 GeV. Detailed information about the design and performance of DELPHI can be found in [11, 12].

In order to select well-measured charged particle tracks, the cuts given in the upper part of Table 1 have been applied. The cuts in the lower part of the table are used to select $e^+e^- \to Z/\gamma \to q\bar{q}$ events and to suppress background processes such as two-photon interactions, beam-gas and beam-wall interactions, leptonic final states, events with hard initial-state radiation (ISR), WW and ZZ pair production.

At energies well above M_Z the high cross-section of the Z resonance raises the probability of events with hard ISR. These "radiative return events" constitute a large fraction of all hadronic events. The initial-state photons are typically aligned along the beam direction and are identified inside the detector only at a rate of about 10% . In order to evaluate the effective hadronic centre-of-mass energy of an event, considering ISR, an algorithm called SPRIME is used [13]. SPRIME is based on a 3C fit imposing transverse momentum and energy conservation. Several assumptions about the event topology are tested. The decision is taken

Table 1. Selection of tracks and events. p is the momentum, Δp its error, r the radial distance to the beam-axis, z the distance to the beam interaction point (I.P.) along the beam-axis, ϕ the azimuthal angle, N_{charged} the number of charged particles, θ_{Thrust} the polar angle of the thrust axis with respect to the beam, E_{tot} the total energy carried by charged and neutral particles, $\sqrt{s'}$ the reconstructed centre-of-mass energy, $\sqrt{s}$ the nominal centre-of-mass energy, and B_{min} is the minimal jet broadening. The first two cuts apply to charged and neutral particles, while the other track selection cuts apply only to charged particles

Track selection	$0.2\,\text{GeV/c} \le p \le 100\,\text{GeV/c}$
	$\Delta p/p \le 1.0$
	measured track length $\ge 30\,\text{cm}$
	distance to I.P in $r\phi$ plane $\le 4\,\text{cm}$
	distance to I.P. in $z \le 10\,\text{cm}$
Event selection	$N_{\text{charged}} \ge 7$
	$25° \le \theta_{\text{Thrust}} \le 155°$
	$E_{\text{tot}} \ge 0.50\sqrt{s}$
	$\sqrt{s'} \ge 90\%\sqrt{s}$
	$N_{\text{charged}} > 500B_{\text{min}} + 1.5$
	$N_{\text{charged}} \le 42$

according to the χ^2 obtained from the constrained fits with different topologies.

Figure 1(left) shows the spectra of the calculated energies for simulated and measured events after all but the
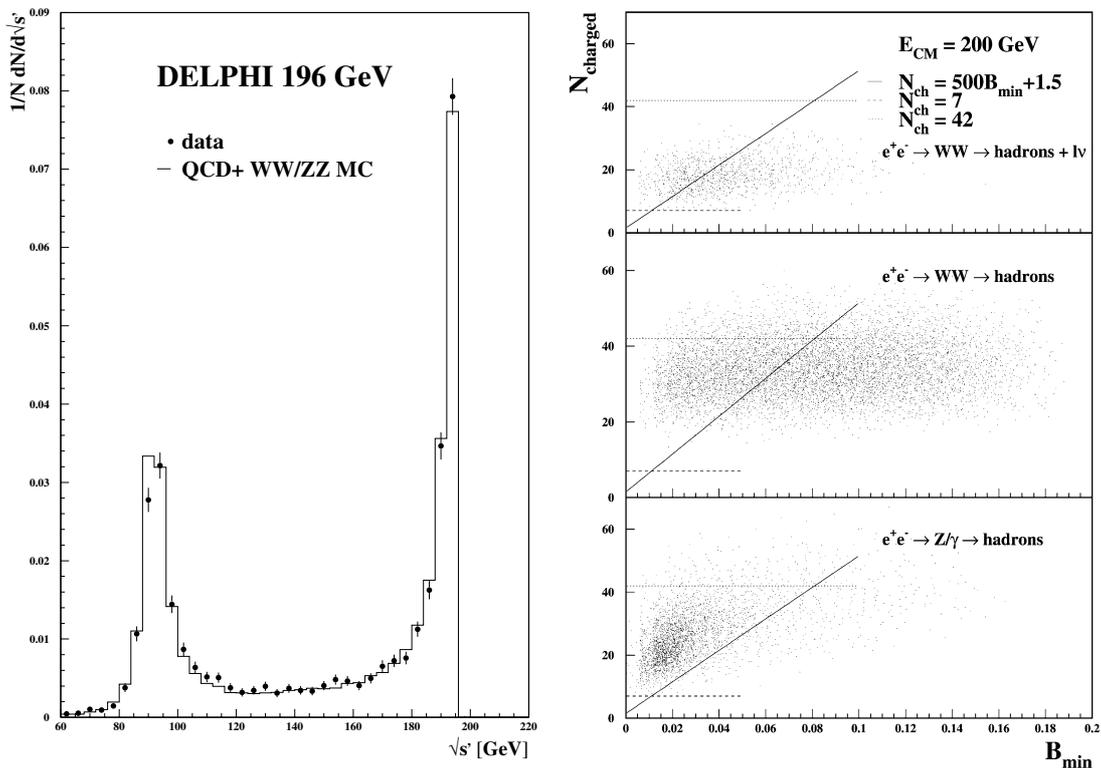

Fig. 1. Left: reconstructed centre-of-mass energy $\sqrt{s'}$. Right: simulation of four-fermion background and QCD events in the N_{charged}-B_{min} plane. The lines delineate the accepted region

Table 2. Luminosities, cross-sections of QCD signal and background from four-fermion events (split into neutral current, NC, and charged current, CC), selection efficiencies, ϵ, and purities, p. The subscript HE denotes QCD high energy events, i.e. with $\sqrt{s'} > 0.9 \cdot \sqrt{s}$. Also given is the total number of selected events and the expected number of remaining four-fermion events

$\sqrt{s}$ [GeV]	183	189	192	196	200	202	205	207
$\mathcal{L}[pb]^{-1}$	55.73	157.97	25.34	67.29	78.07	39.31	76.33	130.12
$\sigma_{\text{tot}}^{\text{QCD}}$[pb]	108.78	100.05	96.06	91.31	86.73	84.56	81.18	79.78
$\sigma_{s'>90\%}^{\text{QCD}}$[pb]	23.09	21.24	20.42	19.36	18.35	18.18	16.89	16.59
$\sigma^{\text{4F,CC}}$[pb]	17.54	18.74	19.10	19.57	19.85	19.97	20.10	20.14
$\sigma^{\text{4F,NC}}$[pb]	8.16	8.15	8.14	8.08	8.03	8.01	7.93	7.90
ϵ_{HE}	0.721	0.720	0.736	0.740	0.735	0.734	0.736	0.749
ϵ_{CC}	0.090	0.100	0.104	0.112	0.122	0.120	0.127	0.124
ϵ_{NC}	0.017	0.017	0.017	0.017	0.015	0.016	0.016	0.016
$p_{HE,QCD}$	0.867	0.848	0.837	0.828	0.808	0.801	0.790	0.795
$\epsilon_{\text{HE}} \cdot p_{\text{HE,QCD}}$	0.625	0.610	0.617	0.612	0.594	0.588	0.581	0.593
# selected events	1070	2848	455	1164	1303	653	1203	2036
# CC background	87.8	296.0	50.1	147.7	189.8	94.1	195.6	315.4
# NC background	7.7	21.4	3.54	9.36	9.65	4.88	9.67	16.60

$\sqrt{s'}$ cut. A cut on the reconstructed centre-of-mass energy $\sqrt{s'} \geq 90\%\sqrt{s}$ is applied to discard radiative return events.

Two-photon events are strongly suppressed by the cuts. Leptonic background was found to be negligible in this analysis as well.

Since the topological signatures of QCD four-jet events and hadronic WW, ZZ and other events with four-fermions (4F) in the final state are similar, no highly efficient separation of QCD events and backgrounds is possible. Furthermore any 4F rejection implies a severe bias to the QCD event shape distributions, which needs to be corrected by simulation.

Our suppression of these backgrounds uses a two-dimensional cut in the plane spanned by the charged particle multiplicity (N_{charged}) and the narrow jet broadening $B_{\min} = \min(B_+, B_-)$. $B_{\pm}$ is defined as the normalized sum over the transverse momentum of charged and neutral particles in the two event hemispheres separated by the plane perpendicular to the thrust axis n_T:

$$B_{\pm} = \left(\sum_{\pm \mathbf{p_i} \cdot \mathbf{n_T} > 0} |\mathbf{p_i} \times \mathbf{n_T}| \right) \bigg/ \left(2 \sum_i |\mathbf{p_i}| \right). \quad (1)$$

By applying a cut on an observable calculated from the narrow event hemisphere only, the bias to event shape observables mainly sensitive to the wide event hemisphere is reduced. The charged particle multiplicity is used to reduce the 4F contribution further. The two-dimensional cut in the N_{charged}-$B_{\min}$ plane exploits the different correlation between these observables for QCD and four-fermion events, as shown in Fig. 1 (right). Especially some reduction for semi-leptonic decaying 4F events is gained. The lines indicate the cut values chosen. This cut suppress almost 90% of the four-fermion background. The remaining 4F

contribution is estimated by the WPHACT [14] generator and subtracted from the measurement.

Table 2 contains the integrated luminosities at different energies, the cross-sections for signal and background and summarizes the selection statistics. The cross-sections were taken from the simulation which was used to correct the data and to subtract the background. The cross-sections for the 4F background are quoted for charged current (CC) and neutral current (NC) contributions separately. Details on the four-fermion simulation in DELPHI can be found in [15].

The influence of detector effects was studied by passing events (generated with $\mathcal{KK}$ [16]) and fragmented with JETSET/PYTHIA [3] using the DELPHI tuning described in [17] through a full detector simulation (DELSIM [11]). This simulation is improved with respect to the previous LEP2 analysis [10] by including electroweak corrections (multiple photon emission, treatment of ISR and FSR etc.). These simulated events are processed with the same reconstruction program and selection cuts as are the real data. In order to correct for cuts, detector, and ISR effects a bin-by-bin acceptance correction C, obtained from $e^+e^- \to Z/\gamma \to q\bar{q}$ simulation, is applied to the data:

$$C_i = \frac{h(f_i)_{\text{gen,noISR}}}{h(f_i)_{\text{acc}}} \quad (2)$$

where $h(f_i)_{\text{gen,noISR}}$ represents bin i of the shape distribution f generated with the tuned generator. The subscript $noISR$ indicates that only events without relevant ISR ($\sqrt{s} - \sqrt{s'} < 0.1\,\text{GeV}$) enter the distribution. $h(f_i)_{\text{acc}}$ represents the accepted distribution f as obtained with the full detector simulation. The more detailed matrix correction used for the data measured at the Z peak [18] is not applied here, because of the smaller statistics at LEP2.
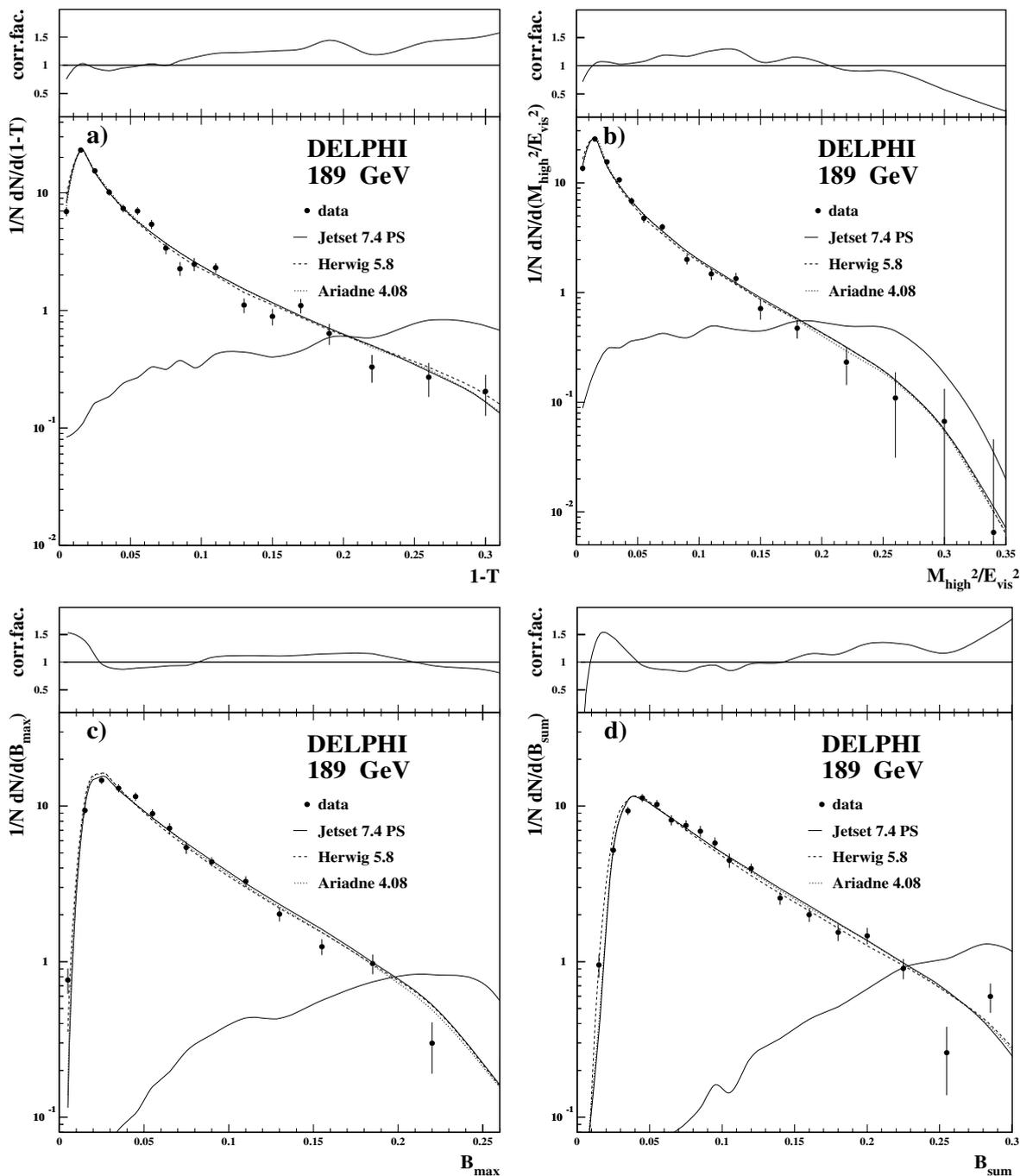
Fig. 2. Event shape distributions of 1-Thrust $(1-T)$, heavy jet mass (M_h^2/E_{vis}^2), wide jet broadening (B_{max}) and total jet broadening (B_{sum}) at 189 GeV. The upper inset shows the acceptance corrections. The central part shows data with statistical uncertainties, simulation and the four-fermion background which was subtracted from the data

3 Event shape distributions and mean values

Selected event shape distributions at 189 and 207 GeV are shown in Figs. 2 and 3. The definitions of these observables are given is Sect. 4.

The data in Figs. 2 and 3 are corrected to be comparable with $e^+e^- \to Z/\gamma \to q\bar{q}$ simulation of charged and neutral hadron production. In the data all charged particles are assumed to have pion mass while neutral particles are considered massless. The monte carlo correction of the

data includes the effects of the simulated particle masses. The Figs. 2 and 3 compare these data with the JETSET [3], ARIADNE [4] and HERWIG [5] generators as tuned by DELPHI [17] with LEP1 data. The amount of 4F-background which was subtracted to obtain the final data points is also shown. The acceptance corrections are plotted in the upper inset.

The Tables 8 and 9 at the end of the paper contain mean values and higher moments for the event shapes 1-T, C parameter, M_h^2/E_{vis}^2, B_{max} and B_{sum}. Also included are
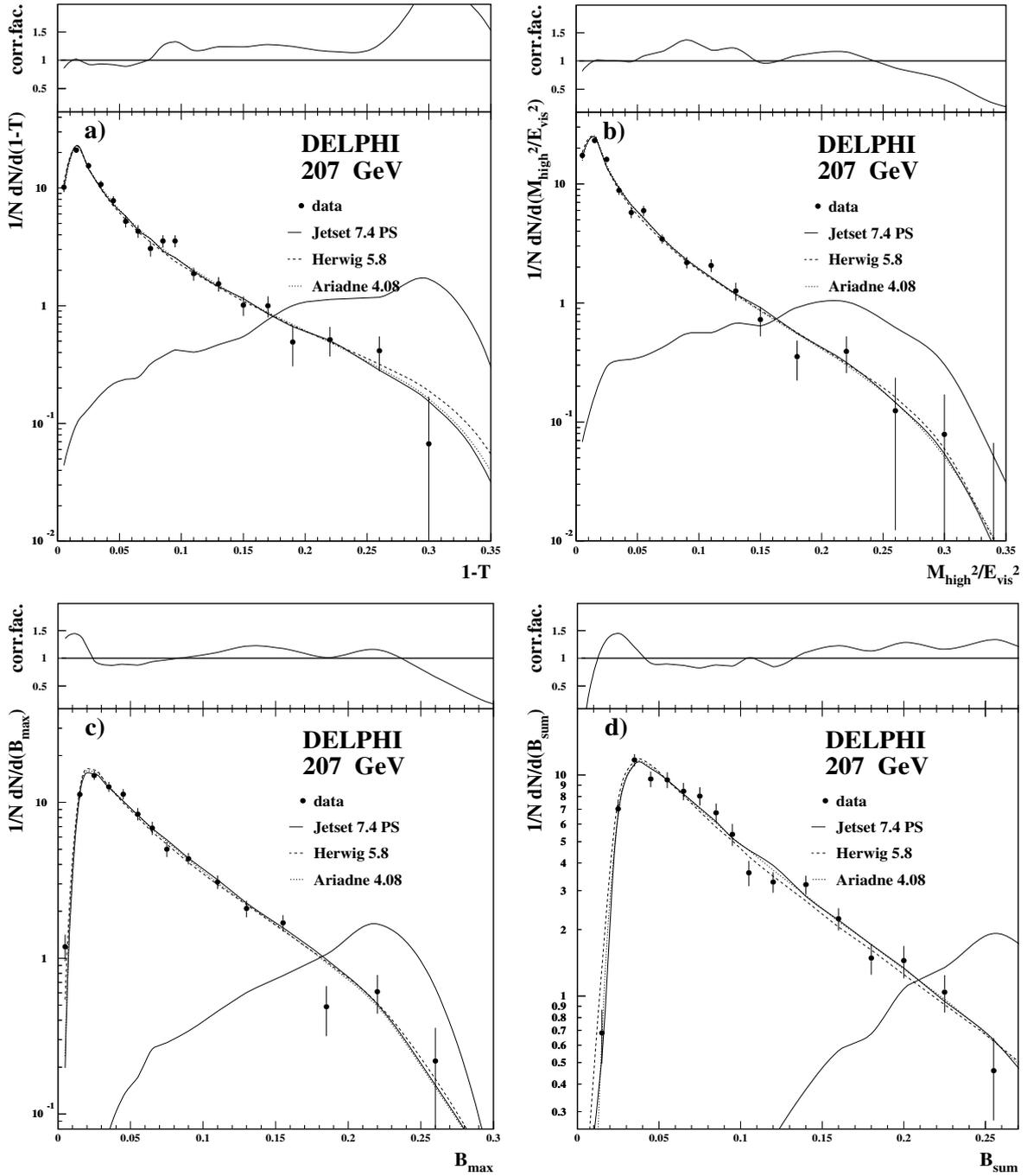
Fig. 3. Event shape distributions of 1-Thrust $(1 - T)$, heavy jet mass $(M_{\rm h}^2/E_{\rm vis}^2)$, wide jet broadening $(B_{\rm max})$ and total jet broadening $(B_{\rm sum})$ at 207 GeV. The upper inset shows the acceptance corrections. The central part shows data with statistical uncertainties, simulation and the four-fermion background which was subtracted from the data

the results for alternative definitions of the heavy jet mass as proposed in [19]. They are obtained if in the definition of the heavy jet mass the invariant mass is calculated with the following replacements:

$$(E_i, \mathbf{p_i}) \rightarrow (|\mathbf{p_i}|, \mathbf{p_i})$$
$$\text{or} \quad (E_i, \mathbf{p_i}) \rightarrow (E_i, E_i \cdot \mathbf{p_i}/|\mathbf{p_i}|).$$

In what follows we will refer to these observables as p-scheme and E-scheme definitions of the heavy jet mass.

In order to estimate the systematic uncertainty from the selection and correction procedure, the effects of the following changes with respect to the standard values have been considered: $N_{\rm ch} \pm 1$, $\Theta_{\rm thrust} \pm 5°$ and $\sqrt{s'}/\sqrt{s} \pm 0.025$. For the 4F cross-section a change of $\pm 5\%$ has been considered and the uncertainty due to the acceptance correction was estimated by a change of ± 0.02. The last uncertainty agrees with that of [17] where the systematic uncertainty was verified using independent data. Half of the difference between up- and downward variation is regarded as

one component of the systematic uncertainty. These five contributions are added in quadrature to estimate the experimental systematic uncertainty.

4 Determination of α_s from event shape distributions

Our determination of α_s is based on the five variables 1-Thrust $(1 - T)$, C-parameter, heavy jet mass $(M_{\mathrm{h}}^2/E_{\mathrm{vis}}^2)$, wide jet broadening (B_{max}) and total jet broadening (B_{sum}). The thrust, T, is defined as:

$$T = \max_{\mathbf{n}} \left\{ \frac{\sum_i |\mathbf{p}_i \cdot \mathbf{n}|}{\sum_i |\mathbf{p}_i|} \right\} = \frac{\sum_i |\mathbf{p}_i \cdot \mathbf{n}_T|}{\sum_i |\mathbf{p}_i|} \; .$$

The vector which maximizes the above expression defines the thrust axis, $\mathbf{n}_T$. The plane perpendicular to the thrust axis divides the event into two hemispheres. Based on this separation several other event shapes can be defined. One defines the heavy jet mass by the following expression:

$$M_{\mathrm{h}}^2/E_{\mathrm{vis}}^2 = \max(M_+^2, M_-^2)/E_{\mathrm{vis}}^2$$

$M_\pm^2$ denotes the invariant mass of the two hemispheres:

$$M_\pm^2 = \left(\sum_{\pm \mathbf{p}_i \cdot \mathbf{n_T} > 0} p_i \right)^2 \; .$$

Here p_i is the four-momentum of the ith particle. Using the expression $B_\pm$ as defined in Equ.1 the wide and total jet broadening are defined as:

$$B_{\mathrm{max}} = \max(B_+, B_-)$$

$$B_{\mathrm{sum}} = B_+ + B_-$$

The linear momentum tensor offers a possibility to define event shapes without distinguishing an event axis. It is defined as:

$$\Theta^{ab} = \sum_{i=1}^{n_{\mathrm{track}}} \frac{p_i^a p_i^b}{|\mathbf{p_i}|} \Bigg/ \sum_{i=1}^{n_{\mathrm{track}}} |\mathbf{p_i}| \qquad \text{with:} \quad a, b = x, y, z$$

From its eigenvalues λ_i the C-parameter is defined:

$$C = 3(\lambda_1\lambda_2 + \lambda_1\lambda_3 + \lambda_2\lambda_3)$$

From these differential distributions α_s is determined by fitting an α_s-dependent QCD prediction folded with a hadronisation correction to the data. The following QCD predictions are used: $\mathcal{O}(\alpha_s^2)$, pure NLLA, and the modified $\mathcal{O}(\alpha_s^2)$+NLLA in the log R-scheme [7–9,20,21]. Hadronisation corrections are calculated using the JETSET PS model (Version 7.4 as tuned by DELPHI [17]). In each bin the QCD prediction is multiplied by the hadronisation correction

$$C_{\mathrm{had}} = \frac{f_{\mathrm{had}}^{\mathrm{Sim.}}}{f_{\mathrm{part}}^{\mathrm{Sim.}}} \quad , \tag{3}$$
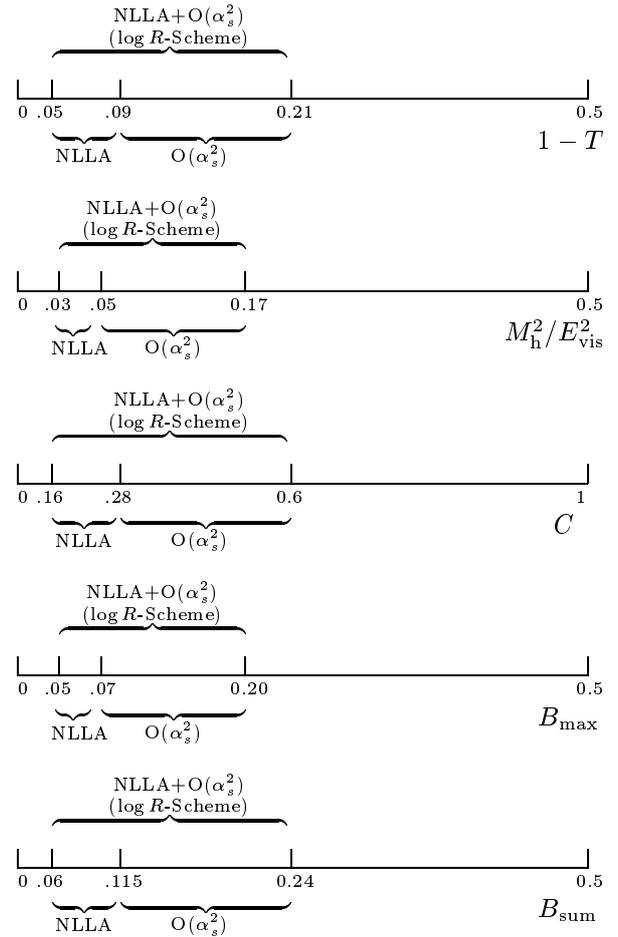
Fig. 4. Fit ranges for the different observables and methods to determine α_s

where $f_{\mathrm{had}}^{\mathrm{Sim.}}$ ($f_{\mathrm{part}}^{\mathrm{Sim.}}$) is the model prediction on hadron (parton) level. The parton level is defined as the final state of the parton shower created by the simulation.

The fit ranges used for the different QCD predictions are shown in Fig. 4. The lower edges are chosen in such a way, that the hadronisation corrections in the 2-jet region remain small ($\leq 10\%$) for LEP2 energies. The upper limit of the fit ranges ensures that the signal-to-background ratio is above 1. The ranges for pure NLLA and $\mathcal{O}(\alpha_s^2)$ fits are chosen to be distinct, so that the results are statistically uncorrelated.

In [18] it has been shown that fixing the renormalisation scale to $\mu = \sqrt{s}$ results in a poor description of the data. Therefore, the experimentally optimized scales (μ_{EOS}) from [18] (see Table 3) are used for the $\mathcal{O}(\alpha_s^2)$ fits. For the NLLA and the combined NLLA+$\mathcal{O}(\alpha_s^2)$ fits, μ is still set equal to $\sqrt{s}$. This is the conventional choice of scale for resummed and matched calculations and allows a direct comparison with the results from other experiments [22]. Furthermore the meaning of the renormalisation scale μ in resummed calculations is different from its interpretation in the framework of fixed-order perturbation theory. While in $\mathcal{O}(\alpha_s^2)$ μ paramatrizes the choice of the renormalisation scheme this interpretation is lost in resummed calculations. This difference makes the application of ex-

Table 3. The values for the experimentally optimized scales from [18]

observable	experimentally optimized scales ($x_\mu = \mu/\sqrt{s}$)
1-T	0.057
C	0.082
$M_{\mathrm{h}}^2/E_{\mathrm{vis}}^2$	0.060
$B_{\max}$	0.143
B_{sum}	0.096

perimentally optimized scales especially for NLLA+$\mathcal{O}(\alpha_s^2)$ predictions meaningless. Tables 10–18 at the end of this paper contain all α_s values derived from event shapes.

4.1 Definition of uncertainties

Experimental systematic uncertainties are obtained from fits to distributions evaluated with different cuts and corrections. These variations are described in Sect. 3. The hadronisation uncertainty is taken to be the bigger of the two differences when the hadronisation correction is determined from the ARIADNE [4] and HERWIG models [5] alternatively. The JETSET result is used as the central value. In all cases the dominant systematics come from the theoretical uncertainty. The conventional method for estimating this uncertainty is to consider the effect of a renormalisation scale variation distributions. This method, however, has at least two drawbacks: since the resulting scale uncertainty is positively correlated with the measured α_s, this definition produces a bias towards small α_s values when combining the results of e.g. different observables. Secondly there are indications that observables calculated only in one hemisphere (like the heavy jet mass or $B_{\max}$) yield less reliable results in the resummation of leading logarithms [23]. This should be reflected in their theoretical uncertainty. Conversely the scale variation yields the smallest uncertainty for the heavy jet mass and especially $B_{\max}$. For these reasons a new definition of the theoretical uncertainty for the logR prediction was developed in cooperation with the LEP QCD working group. By construction, the NLLA calculations do not vanish at the phase-space limit y_{max} [8]. In the so-called modified theory (NLLA or matched) they are forced to vanish by the replacement:

$$L = \ln\frac{1}{y} \rightarrow L = \ln\left[\frac{1}{X \cdot y} - \frac{1}{X \cdot y_{max}} + 1\right].$$

In agreement with the LEP QCD working group y_{max} is chosen as the maximum value of the parton shower simulation [24]. Usually $X = 1$ is chosen for the quantity X, as suggested by the authors of [8], although different values for this X scale introduce only subleading contributions [25]. The theoretical uncertainty of the logR prediction in this analysis is now defined as half of the difference when X is varied between 2/3 and 3/2. By this new definition of the uncertainty the observables $M_{\mathrm{h}}^2/E_{\mathrm{vis}}^2$ and $B_{\max}$, which

are calculated in one hemisphere only, get a bigger uncertainty compared to the uncertainty estimated by μ variation. The same definition of the theoretical uncertainty has been adopted for the pure NLLA prediction.

For the $\mathcal{O}(\alpha_s^2)$ calculation we use, as in the previous publication [10], the effect from the variation around the experimentally optimized scales, μ_{EOS}, between $0.5\mu_{EOS}$ and $2\mu_{EOS}$ to estimate the theoretical uncertainty.

In order to avoid the effect mentioned above of a positive correlation, all scale variations have been calculated for a fixed value of α_s from the theoretical distributions for each method separately. The fixed α_s value is chosen as the average α_s value of the combination. To obtain this value the procedure has to be iterated.

4.2 Method for combining the α_s measurements

For a combination of the α_s results from different observables calculated from the same data sets a proper treatment of the correlation is mandatory. The average value $\bar{y}$ for correlated measurements y_i is [26]:

$$\bar{y} = \sum_{i=1}^{N} w_i y_i \qquad \text{with:} \quad w_i = \frac{\sum_j (V^{-1})_{ij}}{\sum_{k,l}(V^{-1})_{kl}}.$$

Note that the weights w can be negative, if the correlation ρ_{ij} between two quantities i and j is bigger than σ_i/σ_j. Here σ is the uncertainty of the corresponding quantity with $\sigma_i \geq \sigma_j$. The covariance matrix V has an additive structure for each source of uncertainty:

$$V = V^{\mathrm{stat}} + V^{\mathrm{sys.exp.}} + V^{\mathrm{had}} + V^{\mathrm{scale}}.$$

Its statistical component is estimated with simulation which yields correlations of typically $\geq 80\%$. The correlation of systematic uncertainties is modeled by the minimum overlap assumption:

$$V_{ij} = \min(\sigma_i^2, \sigma_j^2).$$

The α_s values evaluated from the distributions and their mean values taking correlations into account are given in the Tables 10–18 at the end of the paper.

5 Determination of α_s from mean values with power corrections

The analytical power ansatz for non-perturbative corrections by Dokshitzer and Webber [6,27] including the Milan factor established by Dokshitzer et al. [28,29] is used to determine α_s from mean event shapes. This ansatz provides an additive term to the perturbative $\mathcal{O}(\alpha_s^2)$ QCD prediction:

$$\langle f \rangle = \frac{1}{\sigma_{\mathrm{tot}}} \int f \frac{df}{d\sigma} d\sigma = \langle f_{\mathrm{pert}} \rangle + \langle f_{\mathrm{pow}} \rangle, \qquad (4)$$

where the 2nd order perturbative prediction can be writ-

ten as

$$\langle f_{\text{pert}} \rangle = A \frac{\alpha_s(\mu)}{2\pi}$$
$$+ \left(A \cdot 2\pi b_0 \log \frac{\mu^2}{s} + (B - 2A) \right) \left(\frac{\alpha_s(\mu)}{2\pi} \right)^2,$$

with A and B being the perturbative coefficients [7,30], μ being the renormalisation scale and $b_0 = (33 - 2N_f)/12\pi$. The power correction is given by

$$\langle f_{\text{pow}} \rangle =$$
$$c_f \frac{4C_F}{\pi^2} \mathcal{M} \frac{\mu_I}{\sqrt{s}}$$
$$\times \left[\alpha_0(\mu_I) - \alpha_s(\mu) - \left(b_0 \cdot \log \frac{\mu^2}{\mu_I^2} + \frac{K}{2\pi} + 2b_0 \right) \alpha_s^2(\mu) \right],$$

where α_0 is a non-perturbative parameter accounting for the contributions to the event shape below an infrared matching scale μ_I and $K = (67/18 - \pi^2/6)C_A - 5N_f/9$. The Milan factor $\mathcal{M}$ is set to 1.49, which corresponds to three active flavours in the non-perturbative region. The observable-dependent quantities A, B and c_f are listed in Table 4. For the jet broadenings c_f takes a more complicated form [31]:

$$c_f = c_B \left(\frac{\pi\sqrt{c_B}}{2\sqrt{C_F \alpha_s(1 + K\frac{\alpha_s}{2\pi})}} + \frac{3}{4} - \frac{2\pi b_0 c_B}{3C_F} + \eta_0 \right) \quad (5)$$

Here c_B is 0.5 or 1 for $\langle B_{\text{max}} \rangle$ or $\langle B_{\text{sum}} \rangle$ respectively, $\eta_0 = -0.6137$. The infrared matching scale is set to $2\,\text{GeV}$ as suggested by the authors of [6], the renormalisation scale

Table 4. A and B coefficients for the expansion of the mean values in $\alpha_s/2\pi$, and values for the observable dependent c_f

observable	A_f	B_f	c_f
$\langle 1 - T \rangle$	2.103	44.99	2
$\langle C \rangle$	8.638	146.8	3π
$\langle M_h^2/E_{vis}^2 \rangle$	2.103	23.24	1
$\langle B_{\text{max}} \rangle$	4.066	-9.53	Eq. (5)
$\langle B_{\text{sum}} \rangle$	4.066	64.24	Eq. (5)

μ is set to $\sqrt{s}$ i.e. the $\overline{MS}$ scheme is used, since the power corrections are provided only in this scheme.

Besides α_s these formulae contain α_0 as the only free parameter. In order to measure α_s from the high energy data this quantity has to be determined. To infer α_0, a combined fit of α_s and α_0 to a large set of measurements at different energies [32] is performed. For $\sqrt{s} \geq M_Z$ only DELPHI measurements are included in the fit. Figure 5 (left) shows the measured mean values of our five observables as a function of the centre-of-mass energy together with the results of the fit. The resulting values of α_0 are summarized in Table 5. The first uncertainty in Table 5 is taken from the fit to the data with full errors, while the second uncertainty reflects the effect of a variation $0.5\mu \leq \mu \leq 2\mu$. Figure 5 (right) shows the fit results also in the α_s-α_0 plane. The extracted α_0 values are supposed to be observable independent and around 0.5 [27, 29]. However, higher order effects are expected to violate this universality. Within the theoretically expected accuracy of 20% this universality is fulfilled.

After fixing α_0 for each observable to the values in Table 5, the α_s values corresponding to the high energy data points can be calculated from (4). The effect of an α_0 variation within its uncertainty was found to be well within the systematic uncertainties of α_s. By using the α_0 value from the global fit, the determination of α_s uses the DELPHI data points twice. But since the global fit is dominated by the low-energy data the effect is negligible. α_s is calculated for all observables individually and then combined taking correlations into account as described in Sect. 4.2. An additional scale uncertainty is calculated by varying μ for a fixed value of α_s and the infrared matching scale μ_I from $1\,\text{GeV}$ to $3\,\text{GeV}$. The α_s results are summarized in the Tables 19 to 22 at the end of the paper. The total error for this method is smaller than e. g. for NLLA+$\mathcal{O}(\alpha_s^2)$ fits. However, the hadron level which is experimentally accessible does include the effects of resonance decays and hadron masses which are not accounted for in the calculation of power corrections. In order to investigate the influence of different hadron level definitions a Monte Carlo study was performed in [19]. Three different hadron level definitions were considered: (i) hadrons which are primary produced, (ii) stable hadrons after resonance decays or (iii) particles out of a subsequent decay into two massless particles. The subsequent determination of the strong coupling from

Table 5. α_0 and α_s values from the global fit of the Dokshitzer-Webber ansatz for mean values to e^+e^- data from several experiments [32]. Only the α_0 values are used further for the α_s determination from single mean values at LEP2

Observable	$\alpha_0(2\,\text{GeV})$	$\alpha_s(M_Z)$	χ^2/ndf
$\langle 1 - T \rangle$	$0.532 \pm 0.011 \pm 0.002$	$0.122 \pm 0.001 \pm 0.009$	69/43
$\langle C \rangle$	$0.442 \pm 0.010 \pm 0.008$	$0.126 \pm 0.002 \pm 0.006$	18/22
$\langle M_h^2/E_{vis}^2 \rangle$	$0.620 \pm 0.028 \pm 0.010$	$0.119 \pm 0.002 \pm 0.004$	10/32
$\langle M_h^2/E_{vis}^2 \rangle$ (E def)	$0.576 \pm 0.113 \pm 0.002$	$0.111 \pm 0.005 \pm 0.003$	5/14
$\langle M_h^2/E_{vis}^2 \rangle$ (p def)	$0.517 \pm 0.110 \pm 0.003$	$0.110 \pm 0.005 \pm 0.004$	3/14
$\langle B_{\text{max}} \rangle$	$0.460 \pm 0.029 \pm 0.078$	$0.116 \pm 0.001 \pm 0.002$	7/22
$\langle B_{\text{sum}} \rangle$	$0.452 \pm 0.014 \pm 0.015$	$0.118 \pm 0.001 \pm 0.004$	12/22
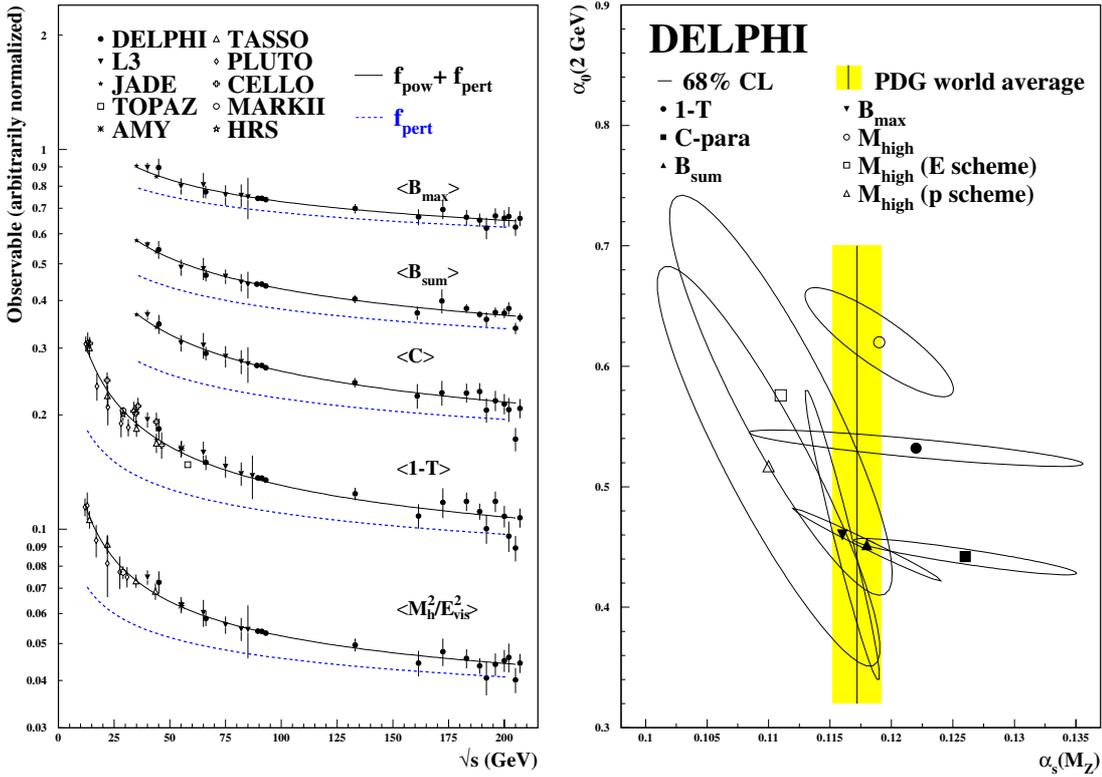
Fig. 5. Left: Dokshitzer-Webber fit to several mean values. The dotted line shows the perturbative contribution. Right: the results of the global fits in the α_s-α_0 plane. The vertical line with shading shows the world average of α_s

Table 6. Results for the slope b when fitting the function $1/(b \log \sqrt{s} + c)$ to α_s values obtained for the different energies. Also given is the corresponding result for the number of active flavours, N_F

theory used for measurement	$\frac{d\alpha_s^{-1}}{d\log\sqrt{s}} \pm$ stat $\pm$ sys	χ^2/ndf	N_F
mean values + power corr.	$1.11 \pm 0.09 \pm 0.19$	1.25	6.3 ± 1.7
$\mathcal{O}(\alpha_s^2)$+NLLA (logR)	$1.32 \pm 0.11 \pm 0.27$	0.58	4.6 ± 2.3
$\mathcal{O}(\alpha_s^2)$	$1.27 \pm 0.15 \pm 0.33$	0.29	5.0 ± 2.9
NLLA	$1.40 \pm 0.17 \pm 0.44$	0.83	4.0 ± 3.8
QCD expectation	1.27		5

Table 7. Results of combining all DELPHI α_s measurements at LEP1 and LEP2. For the α_s results from mean values with power corrections "hadronisation uncertainty" (had.) denotes the combined effect of the μ_I variation and the uncertainty related to resonance decays and particle masses as described at the end of Sect. 5. The scale uncertainty is either the effect of a variation of the renormalisation scale μ ($\mathcal{O}(\alpha_s^2)$ and power corrections) or the effect of changing the X scale (see Sect. 4.1)

theory	$\alpha_s(M_Z)$	stat.	sys.exp.	had.	scale	tot
mean values + power corr.	0.1184	0.0004	0.0008	0.0022	0.0031	0.0039
$\mathcal{O}(\alpha_s^2)$+NLLA (logR)	0.1205	0.0010	0.0018	0.0013	0.0048	0.0054
$\mathcal{O}(\alpha_s^2)$	0.1157	0.0008	0.0016	0.0016	0.0022	0.0033
NLLA	0.1093	0.0012	0.0020	0.0011	0.0050	0.0056

Table 8. Mean values and higher moments of the Thrust, C, B_{max} and B_{sum} distributions with statistical and systematic errors

$\sqrt{s}$	$\langle 1-T \rangle$	$\langle (1-T)^2 \rangle$	$\langle (1-T)^3 \rangle$
183	$0.0592 \pm 0.0024 \pm 0.0020$	$0.00766 \pm 0.00070 \pm 0.00054$	$0.00154 \pm 0.00021 \pm 0.00015$
189	$0.0557 \pm 0.0016 \pm 0.0022$	$0.00658 \pm 0.00048 \pm 0.00060$	$0.00121 \pm 0.00015 \pm 0.00017$
192	$0.0502 \pm 0.0040 \pm 0.0023$	$0.00454 \pm 0.00116 \pm 0.00064$	$0.00055 \pm 0.00035 \pm 0.00018$
196	$0.0592 \pm 0.0029 \pm 0.0024$	$0.00810 \pm 0.00085 \pm 0.00067$	$0.00171 \pm 0.00026 \pm 0.00019$
200	$0.0541 \pm 0.0028 \pm 0.0025$	$0.00613 \pm 0.00086 \pm 0.00071$	$0.00101 \pm 0.00027 \pm 0.00020$
202	$0.0480 \pm 0.0040 \pm 0.0025$	$0.00330 \pm 0.00121 \pm 0.00072$	$0.00003 \pm 0.00039 \pm 0.00020$
205	$0.0446 \pm 0.0030 \pm 0.0026$	$0.00322 \pm 0.00090 \pm 0.00077$	$0.00019 \pm 0.00027 \pm 0.00022$
207	$0.0536 \pm 0.0023 \pm 0.0027$	$0.00572 \pm 0.00066 \pm 0.00079$	$0.00086 \pm 0.00020 \pm 0.00022$
	$\langle C \rangle$	$\langle (C)^2 \rangle$	$\langle (C)^3 \rangle$
183	$0.2286 \pm 0.0070 \pm 0.0106$	$0.08846 \pm 0.00544 \pm 0.00952$	$0.04585 \pm 0.00413 \pm 0.00824$
189	$0.2304 \pm 0.0046 \pm 0.0113$	$0.09252 \pm 0.00369 \pm 0.01030$	$0.05114 \pm 0.00287 \pm 0.00894$
192	$0.2060 \pm 0.0115 \pm 0.0117$	$0.06634 \pm 0.00915 \pm 0.01073$	$0.02676 \pm 0.00716 \pm 0.00933$
196	$0.2181 \pm 0.0080 \pm 0.0121$	$0.08091 \pm 0.00657 \pm 0.01118$	$0.03909 \pm 0.00515 \pm 0.00973$
200	$0.2139 \pm 0.0079 \pm 0.0126$	$0.07882 \pm 0.00658 \pm 0.01170$	$0.03907 \pm 0.00524 \pm 0.01020$
202	$0.2066 \pm 0.0111 \pm 0.0127$	$0.06730 \pm 0.00919 \pm 0.01184$	$0.02761 \pm 0.00737 \pm 0.01032$
205	$0.1726 \pm 0.0088 \pm 0.0133$	$0.03792 \pm 0.00743 \pm 0.01251$	$0.00349 \pm 0.00596 \pm 0.01092$
207	$0.2081 \pm 0.0065 \pm 0.0136$	$0.07123 \pm 0.00540 \pm 0.01278$	$0.03150 \pm 0.00426 \pm 0.01116$
	$\langle B_{\mathrm{sum}} \rangle$	$\langle (B_{\mathrm{sum}})^2 \rangle$	$\langle (B_{\mathrm{sum}})^3 \rangle$
183	$0.0953 \pm 0.0023 \pm 0.0010$	$0.01334 \pm 0.00070 \pm 0.00028$	$0.00247 \pm 0.00020 \pm 0.00011$
189	$0.0920 \pm 0.0015 \pm 0.0010$	$0.01192 \pm 0.00047 \pm 0.00030$	$0.00199 \pm 0.00013 \pm 0.00012$
192	$0.0893 \pm 0.0038 \pm 0.0010$	$0.01113 \pm 0.00117 \pm 0.00031$	$0.00178 \pm 0.00034 \pm 0.00013$
196	$0.0931 \pm 0.0026 \pm 0.0010$	$0.01266 \pm 0.00082 \pm 0.00032$	$0.00224 \pm 0.00024 \pm 0.00014$
200	$0.0927 \pm 0.0026 \pm 0.0010$	$0.01254 \pm 0.00081 \pm 0.00034$	$0.00222 \pm 0.00023 \pm 0.00015$
202	$0.0954 \pm 0.0035 \pm 0.0010$	$0.01344 \pm 0.00111 \pm 0.00034$	$0.00257 \pm 0.00032 \pm 0.00015$
205	$0.0845 \pm 0.0028 \pm 0.0010$	$0.00952 \pm 0.00086 \pm 0.00036$	$0.00131 \pm 0.00025 \pm 0.00016$
207	$0.0902 \pm 0.0021 \pm 0.0010$	$0.01151 \pm 0.00066 \pm 0.00036$	$0.00188 \pm 0.00019 \pm 0.00016$
	$\langle B_{\mathrm{max}} \rangle$	$\langle (B_{\mathrm{max}})^2 \rangle$	$\langle (B_{\mathrm{max}})^3 \rangle$
183	$0.0663 \pm 0.0021 \pm 0.0021$	$0.00688 \pm 0.00053 \pm 0.00034$	$0.00095 \pm 0.00013 \pm 0.00007$
189	$0.0652 \pm 0.0014 \pm 0.0022$	$0.00656 \pm 0.00037 \pm 0.00036$	$0.00089 \pm 0.00009 \pm 0.00008$
192	$0.0621 \pm 0.0035 \pm 0.0022$	$0.00557 \pm 0.00096 \pm 0.00038$	$0.00061 \pm 0.00026 \pm 0.00008$
196	$0.0668 \pm 0.0024 \pm 0.0022$	$0.00719 \pm 0.00064 \pm 0.00039$	$0.00105 \pm 0.00016 \pm 0.00009$
200	$0.0659 \pm 0.0024 \pm 0.0023$	$0.00699 \pm 0.00063 \pm 0.00041$	$0.00100 \pm 0.00016 \pm 0.00009$
202	$0.0666 \pm 0.0033 \pm 0.0023$	$0.00671 \pm 0.00089 \pm 0.00041$	$0.00087 \pm 0.00023 \pm 0.00009$
205	$0.0625 \pm 0.0025 \pm 0.0023$	$0.00585 \pm 0.00068 \pm 0.00044$	$0.00073 \pm 0.00017 \pm 0.00010$
207	$0.0658 \pm 0.0020 \pm 0.0023$	$0.00695 \pm 0.00053 \pm 0.00044$	$0.00100 \pm 0.00013 \pm 0.00010$

power corrections leads to a shift in α_s of ± 0.0035 with respect to the hadron level (ii). With regard to these extreme assumptions one may therefore assign $0.007/\sqrt{12} = 0.002$ as an additional uncertainty which accounts for the fact that resonance decays and hadron masses are not considered in the calculation.

6 The running of α_s

The α_s values determined at different energies are used to test the predicted scale dependence of the coupling. We include also the LEP2 results at 133, 161 and 172 GeV from [10]. For α_s at and around M_Z we have reanalyzed the distributions from [10] for the five observables and combined the results using the same treatment of correla-

Table 9. Mean values and higher moments for the M_h^2/E_{vis}^2 distributions in the standard, E-scheme and p-scheme definitions with statistical and systematic errors

$\sqrt{s}$	$\langle M_{\mathrm{h}}^2/E_{\mathrm{vis}}^2 \rangle$	$\langle (M_{\mathrm{h}}^2/E_{\mathrm{vis}}^2)^2 \rangle$	$\langle (M_{\mathrm{h}}^2/E_{\mathrm{vis}}^2)^3 \rangle$
183	$0.0457 \pm 0.0023 \pm 0.0012$	$0.00451 \pm 0.00066 \pm 0.00027$	$0.00068 \pm 0.00021 \pm 0.00006$
189	$0.0437 \pm 0.0016 \pm 0.0013$	$0.00408 \pm 0.00045 \pm 0.00030$	$0.00060 \pm 0.00014 \pm 0.00007$
192	$0.0406 \pm 0.0039 \pm 0.0013$	$0.00285 \pm 0.00117 \pm 0.00032$	$0.00024 \pm 0.00040 \pm 0.00008$
196	$0.0441 \pm 0.0027 \pm 0.0014$	$0.00421 \pm 0.00079 \pm 0.00034$	$0.00060 \pm 0.00024 \pm 0.00008$
200	$0.0451 \pm 0.0027 \pm 0.0015$	$0.00458 \pm 0.00078 \pm 0.00036$	$0.00071 \pm 0.00025 \pm 0.00009$
202	$0.0460 \pm 0.0038 \pm 0.0015$	$0.00470 \pm 0.00112 \pm 0.00036$	$0.00083 \pm 0.00037 \pm 0.00009$
205	$0.0401 \pm 0.0028 \pm 0.0016$	$0.00338 \pm 0.00080 \pm 0.00039$	$0.00045 \pm 0.00023 \pm 0.00009$
207	$0.0444 \pm 0.0022 \pm 0.0016$	$0.00439 \pm 0.00066 \pm 0.00040$	$0.00068 \pm 0.00021 \pm 0.00010$
	$\langle M_{\mathrm{h}}^2/E_{\mathrm{vis}}^2 p \rangle$	$\langle (M_{\mathrm{h}}^2/E_{\mathrm{vis}}^2 p)^2 \rangle$	$\langle (M_{\mathrm{h}}^2/E_{\mathrm{vis}}^2 p)^3 \rangle$
183	$0.0427 \pm 0.0023 \pm 0.0012$	$0.00421 \pm 0.00066 \pm 0.00027$	$0.00068 \pm 0.00021 \pm 0.00006$
189	$0.0411 \pm 0.0016 \pm 0.0013$	$0.00383 \pm 0.00045 \pm 0.00030$	$0.00060 \pm 0.00014 \pm 0.00007$
192	$0.0384 \pm 0.0039 \pm 0.0013$	$0.00274 \pm 0.00117 \pm 0.00032$	$0.00025 \pm 0.00039 \pm 0.00008$
196	$0.0413 \pm 0.0027 \pm 0.0014$	$0.00396 \pm 0.00079 \pm 0.00034$	$0.00057 \pm 0.00024 \pm 0.00008$
200	$0.0424 \pm 0.0027 \pm 0.0015$	$0.00426 \pm 0.00078 \pm 0.00036$	$0.00065 \pm 0.00025 \pm 0.00009$
202	$0.0436 \pm 0.0038 \pm 0.0015$	$0.00451 \pm 0.00112 \pm 0.00036$	$0.00081 \pm 0.00037 \pm 0.00009$
205	$0.0380 \pm 0.0029 \pm 0.0016$	$0.00320 \pm 0.00080 \pm 0.00039$	$0.00043 \pm 0.00023 \pm 0.00009$
207	$0.0420 \pm 0.0023 \pm 0.0016$	$0.00419 \pm 0.00067 \pm 0.00040$	$0.00065 \pm 0.00021 \pm 0.00010$
	$\langle M_{\mathrm{h}}^2/E_{\mathrm{vis}}^2 E \rangle$	$\langle (M_{\mathrm{h}}^2/E_{\mathrm{vis}}^2 E)^2 \rangle$	$\langle (M_{\mathrm{h}}^2/E_{\mathrm{vis}}^2 E)^3 \rangle$
183	$0.0434 \pm 0.0023 \pm 0.0012$	$0.00426 \pm 0.00066 \pm 0.00027$	$0.00064 \pm 0.00021 \pm 0.00006$
189	$0.0417 \pm 0.0016 \pm 0.0013$	$0.00390 \pm 0.00045 \pm 0.00030$	$0.00057 \pm 0.00014 \pm 0.00007$
192	$0.0391 \pm 0.0039 \pm 0.0013$	$0.00282 \pm 0.00117 \pm 0.00032$	$0.00026 \pm 0.00039 \pm 0.00008$
196	$0.0420 \pm 0.0027 \pm 0.0014$	$0.00403 \pm 0.00079 \pm 0.00034$	$0.00058 \pm 0.00024 \pm 0.00008$
200	$0.0430 \pm 0.0027 \pm 0.0015$	$0.00434 \pm 0.00078 \pm 0.00036$	$0.00067 \pm 0.00025 \pm 0.00009$
202	$0.0440 \pm 0.0038 \pm 0.0015$	$0.00450 \pm 0.00112 \pm 0.00036$	$0.00080 \pm 0.00037 \pm 0.00009$
205	$0.0385 \pm 0.0029 \pm 0.0016$	$0.00325 \pm 0.00080 \pm 0.00039$	$0.00044 \pm 0.00023 \pm 0.00009$
207	$0.0426 \pm 0.0023 \pm 0.0016$	$0.00425 \pm 0.00067 \pm 0.00040$	$0.00066 \pm 0.00021 \pm 0.00010$

tions as described in Sect. 4.2. For α_s from mean values the measurements of events with reduced centre-of-mass energy between 44 and 76 GeV [33] and the data between 133 and 172 GeV [10] have been included as well. In the Tables 10–22 at the end of this paper all these α_s values are provided.

The logarithmic energy slope of the inverse coupling is given by:

$$\frac{\mathrm{d}\alpha_s^{-1}}{\mathrm{d}\log\sqrt{s}} = 2b_0 + 2b_1\alpha_s + \dots, \qquad (6)$$

with $b_0 = \frac{33-2N_f}{12\pi}$ and $b_1 = \frac{153-19N_f}{24\pi^2}$ corresponding to the first coefficients of the β function. The measurement of this quantity allows both a test of QCD and a consistency check of the four different methods used to determine α_s. Equation 6 shows that in leading order $\mathrm{d}\alpha_s^{-1}/\mathrm{d}\log\sqrt{s}$ is independent of α_s and twice the first coefficient of the β function. Evaluating this equation in second order results in a slight

dependence on α_s. With α_s=0.11 (which corresponds to $\Lambda_{QCD} = 230$ MeV and $\sqrt{s}$ =150 GeV, the average energy of our measurements) one obtains $\mathrm{d}\alpha_s^{-1}/\mathrm{d}\log\sqrt{s} = 1.27$.

Table 6 gives the slopes when fitting the function $(b\log\sqrt{s} + c)$ to the α_s^{-1} values. The correlation between the α_s measurements is taken into account by including the full covariance matrix in the definition of the χ^2 function. The correlation is modeled as described in Sect. 4.2. The only difference here is that the statistical uncertainties are uncorrelated. The α_s values and the fit of their energy dependence are also displayed in Fig. 6. The results are in good agreement with the QCD expectation. Using the definition of the b_i the result for the slope can be converted into the number of active flavours, N_f. These numbers are also included in Table 6.

A model-independent way to measure the β function is offered by applying the renormalisation group invariant (RGI) perturbation theory to the mean values of event shapes directly [33].
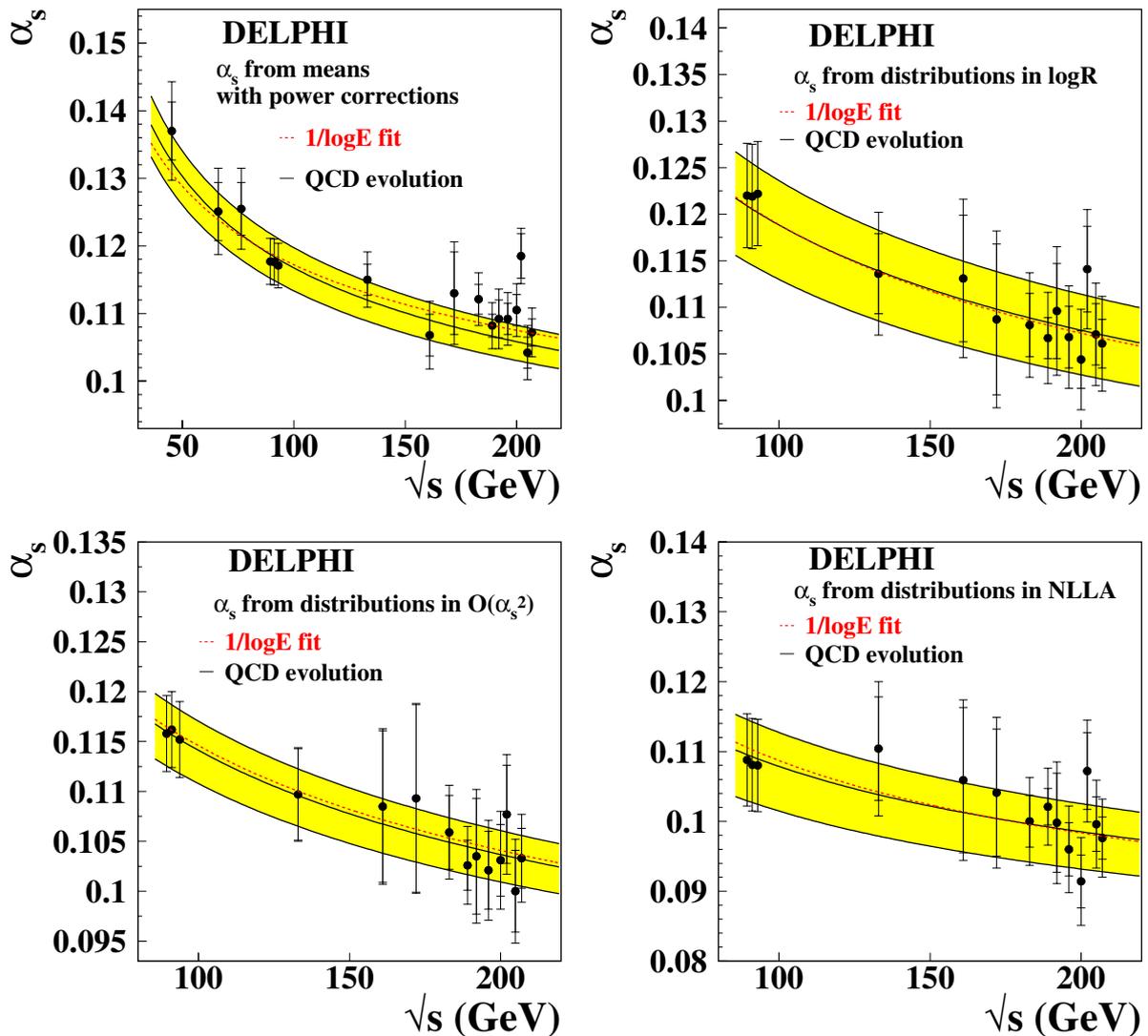
Fig. 6. Energy dependence of α_s as obtained from event shape distributions using different theoretical calculations. The total and statistical (inner error-bars) uncertainties are shown. The band displays the average values of these measurements when extrapolated according to the QCD prediction. The dashed lines show the result of the $1/\log\sqrt{s}$ fit

7 Combination of all DELPHI α_s measurements

As shown in the last section, the energy dependence of α_s is shown to be in good agreement with the QCD prediction. Assuming now the validity of QCD, all α_s results can be evolved to a reference energy, e.g. M_Z, and combined to a single $\alpha_s(M_Z)$ measurement. Again we include results from other LEP2 energies and LEP1 as described in Sect. 6. Combining the α_s results is, again, complicated by correlations among these measurements. Although the measurements at different energies are clearly statistically independent, the systematic and theoretical uncertainties are not. Again this part of the covariance matrix was modeled assuming minimum overlap.

The results of the combinations are given in Table 7 and displayed in Fig. 7. The figure contains in brackets also the weights of the individual measurements within the average. As can be seen from these numbers the weight of LEP1 and

LEP2 measurements are roughly the same, since smaller theoretical uncertainties at LEP2 compensate for the larger statistical error. As can be seen from Table 7 the total error is still dominated by the scale uncertainty. The result with the smallest total uncertainty is deduced from the $\mathcal{O}(\alpha_s^2)$ prediction from distributions. Here the total uncertainty is 0.0033. This value can be compared with the central result of the DELPHI analysis [18] from the observable jet cone energy fraction (JCEF) alone: α_s=0.1180±0.0018. The different precision is mainly due to the definition of the scale uncertainty. While we use the variation $0.5\mu \leq \mu \leq 2\mu$, the analysis [18] changes the corresponding quantity only between $\sqrt{0.5}\mu$ and $\sqrt{2}\mu$. The actual choice of the μ variation is not guided by solid theoretical arguments and was studied in all possible detail in [18]. However, our definition of the theoretical uncertainty yields good agreement with the average root-mean-square of the fits to the five different observables at the same energy (see Tables 10–12). Another reason for the higher precision in [18] is the use of the ob-
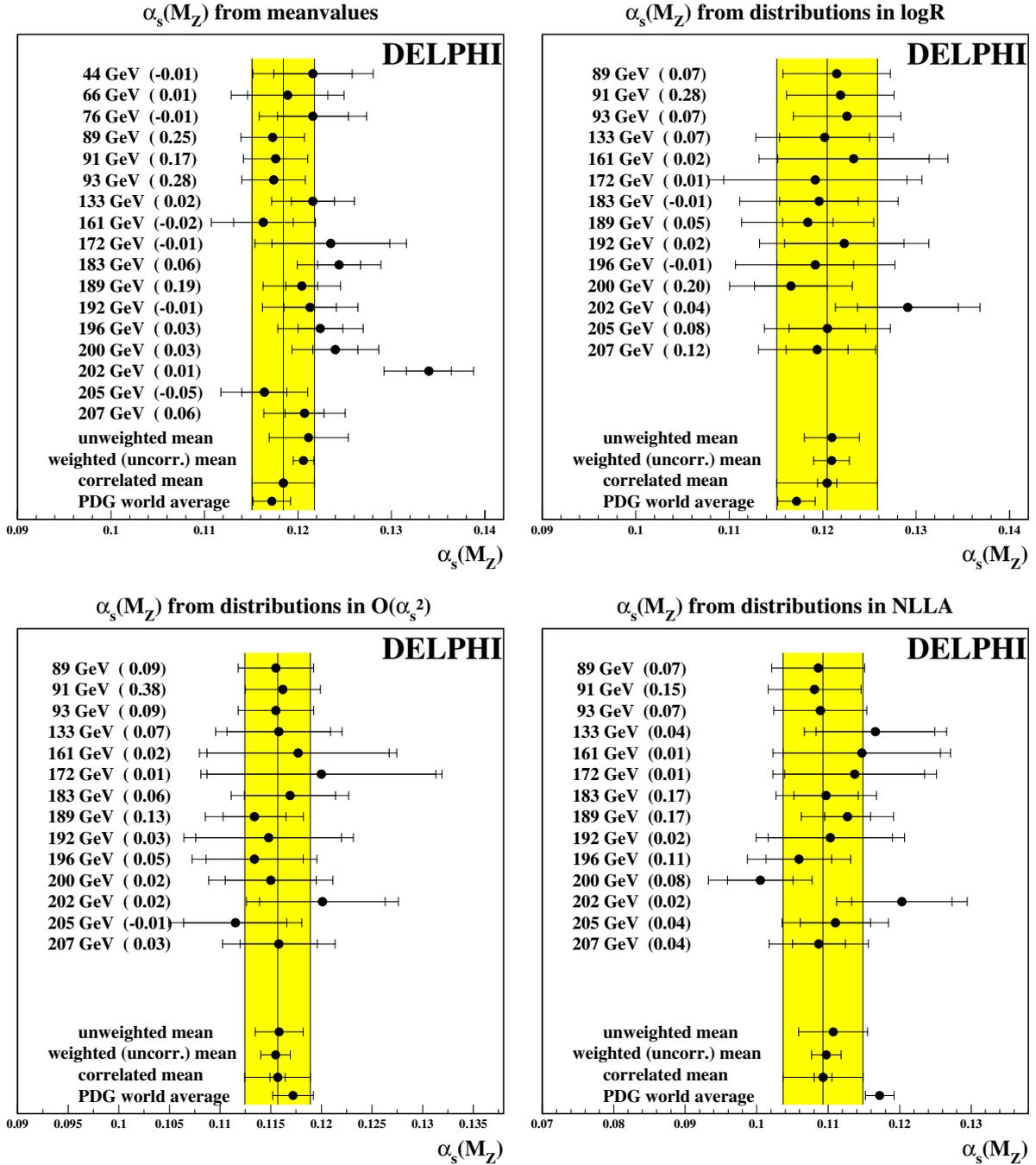
Fig. 7. Results of combining all DELPHI α_s measurements at LEP1 and LEP2. The total and statistical (inner error-bars) uncertainties of the individual measurements are displayed. The central results are the correlated means. For comparison also the unweighted and total-error weighted (but uncorrelated) averages are shown. For the unweighted mean the size of the error-bars indicate the RMS of the measurements. The weights of the individual measurements within the correlated average are given in brackets. Note that these can turn negative in the presence of strong correlation as e.g. for the α_s results from mean values

servable JCEF, which has particularly small uncertainties from hadronisation and scale variation. However, the focus of this work is the analysis of five observables with several different techniques. At present the theoretical uncertainties of α_s measurements from event shape distributions are subject of a debate. Further substantial progress can only be achieved by the arrival of next-to-next-to-leading-order (NNLO) calculations.

8 Conclusion

A measurement of event shape distributions and mean values is presented as obtained from data at centre-of-mass energies from 183 to 207 GeV. The strong coupling constant α_s has been determined from the event shape variables Thrust, C parameter, heavy jet mass, wide and total jet broadening, with four different methods: the differential

Table 10. Results of α_s measurements from distributions in $\mathcal{O}(\alpha_s^2)$. The data of [10] have been reanalyzed for this analysis

observable	α_s in $\mathcal{O}(\alpha_s^2)$					
	1-T	C	M_h^2/E_{vis}^2	B_{max}	B_{sum}	average
fit range	0.09–0.21	0.28–0.6	0.05–0.17	0.07–0.20	0.115–0.24	
α_s(89.5 GeV)	0.1135	0.1149	0.1222	0.1186	0.1123	0.1158
$\pm\Delta$ stat.	0.0004	0.0004	0.0005	0.0005	0.0003	0.0004
$\pm\Delta$ sys. exp.	0.0009	0.0021	0.0014	0.0022	0.0030	0.0015
$\pm\Delta$ had.	0.0026	0.0023	0.0025	0.0031	0.0032	0.0027
$\pm\Delta$ μ_R scale	0.0040	0.0054	0.0040	0.0018	0.0068	0.0022
$\pm\Delta_{tot}$	0.0049	0.0062	0.0051	0.0042	0.0081	0.0038
					RMS	0.0040
α_s(91.2 GeV)	0.1139	0.1155	0.1230	0.1191	0.1128	0.1162
$\pm\Delta$ stat.	0.0002	0.0002	0.0002	0.0002	0.0002	0.0002
$\pm\Delta$ sys. exp.	0.0009	0.0021	0.0014	0.0022	0.0030	0.0015
$\pm\Delta$ had.	0.0026	0.0023	0.0025	0.0031	0.0032	0.0027
$\pm\Delta$ μ_R scale	0.0040	0.0054	0.0040	0.0018	0.0068	0.0022
$\pm\Delta_{tot}$	0.0049	0.0062	0.0051	0.0042	0.0081	0.0038
					RMS	0.0042
α_s(93.0 GeV)	0.1128	0.1140	0.1208	0.1179	0.1117	0.1152
$\pm\Delta$ stat.	0.0004	0.0004	0.0005	0.0005	0.0003	0.0003
$\pm\Delta$ sys. exp.	0.0009	0.0021	0.0014	0.0022	0.0030	0.0015
$\pm\Delta$ had.	0.0026	0.0023	0.0025	0.0031	0.0032	0.0027
$\pm\Delta$ μ_R scale	0.0040	0.0054	0.0040	0.0018	0.0068	0.0022
$\pm\Delta_{tot}$	0.0049	0.0062	0.0051	0.0042	0.0081	0.0038
					RMS	0.0039

Table 11. Results of α_s measurements from distributions in $\mathcal{O}(\alpha_s^2)$

observable	α_s in $\mathcal{O}(\alpha_s^2)$					
	1-T	C	M_h^2/E_{vis}^2	B_{max}	B_{sum}	average
fit range	0.09–0.21	0.28–0.6	0.05–0.17	0.07–0.20	0.115–0.24	
α_s(183 GeV)	0.1075	0.1053	0.1053	0.1065	0.1024	0.1059
$\pm\Delta$ stat.	0.0042	0.0039	0.0047	0.0044	0.0034	0.0037
$\pm\Delta$ sys. exp.	0.0022	0.0023	0.0024	0.0026	0.0012	0.0020
$\pm\Delta$ had.	0.0015	0.0010	0.0033	0.0003	0.0009	0.0008
$\pm\Delta$ μ_R scale	0.0030	0.0033	0.0030	0.0013	0.0050	0.0020
$\pm\Delta_{tot}$	0.0058	0.0057	0.0069	0.0053	0.0062	0.0047
					RMS	0.0019
α_s(189 GeV)	0.1000	0.1038	0.1056	0.1042	0.1007	0.1026
$\pm\Delta$ stat.	0.0030	0.0025	0.0030	0.0028	0.0022	0.0025
$\pm\Delta$ sys. exp.	0.0024	0.0023	0.0024	0.0028	0.0012	0.0022
$\pm\Delta$ had.	0.0010	0.0014	0.0032	0.0005	0.0011	0.0007
$\pm\Delta$ μ_R scale	0.0029	0.0032	0.0029	0.0013	0.0050	0.0018
$\pm\Delta_{tot}$	0.0049	0.0049	0.0058	0.0042	0.0057	0.0039
					RMS	0.0024
α_s(192 GeV)	0.1047	0.1053	0.1143	0.1079	0.1029	0.1035
$\pm\Delta$ stat.	0.0072	0.0064	0.0074	0.0073	0.0055	0.0058
$\pm\Delta$ sys. exp.	0.0026	0.0024	0.0025	0.0029	0.0012	0.0019
$\pm\Delta$ had.	0.0003	0.0009	0.0030	0.0004	0.0006	0.0006
$\pm\Delta$ μ_R scale	0.0029	0.0032	0.0029	0.0013	0.0050	0.0028
$\pm\Delta_{tot}$	0.0081	0.0076	0.0088	0.0079	0.0076	0.0067
					RMS	0.0044
α_s(196 GeV)	0.0977	0.1041	0.1086	0.1034	0.1016	0.1021
$\pm\Delta$ stat.	0.0050	0.0041	0.0041	0.0046	0.0036	0.0039
$\pm\Delta$ sys. exp.	0.0027	0.0024	0.0024	0.0030	0.0012	0.0021
$\pm\Delta$ had.	0.0011	0.0009	0.0038	0.0003	0.0005	0.0005
$\pm\Delta$ μ_R scale	0.0029	0.0032	0.0029	0.0013	0.0049	0.0023
$\pm\Delta_{tot}$	0.0065	0.0058	0.0072	0.0057	0.0062	0.0050
					RMS	0.0039

Table 12. Results of α_s measurements from distributions in $\mathcal{O}(\alpha_s^2)$

observable	α_s in $\mathcal{O}(\alpha_s^2)$					
	1-T	C	$M_{\mathrm{h}}^2/E_{\mathrm{vis}}^2$	B_{max}	B_{sum}	average
fit range	0.09–0.21	0.28–0.6	0.05–0.17	0.07–0.20	0.115–0.24	
α_s (200 GeV)	0.1074	0.1039	0.1085	0.1026	0.1032	0.1031
$\pm\Delta$ stat.	0.0042	0.0039	0.0045	0.0044	0.0034	0.0036
$\pm\Delta$ sys. exp.	0.0028	0.0025	0.0026	0.0031	0.0012	0.0022
$\pm\Delta$ had.	0.0014	0.0015	0.0032	0.0006	0.0011	0.0009
$\pm\Delta$ μ_R scale	0.0029	0.0032	0.0029	0.0013	0.0049	0.0023
$\pm\Delta_{\mathrm{tot}}$	0.0060	0.0058	0.0068	0.0055	0.0062	0.0049
					RMS	0.0027
α_s (202 GeV)	0.1054	0.1107	0.1169	0.1114	0.1055	0.1077
$\pm\Delta$ stat.	0.0064	0.0052	0.0062	0.0061	0.0047	0.0049
$\pm\Delta$ sys. exp.	0.0028	0.0025	0.0026	0.0031	0.0012	0.0020
$\pm\Delta$ had.	0.0016	0.0009	0.0034	0.0004	0.0005	0.0007
$\pm\Delta$ μ_R scale	0.0029	0.0031	0.0029	0.0013	0.0049	0.0026
$\pm\Delta_{\mathrm{tot}}$	0.0077	0.0066	0.0080	0.0070	0.0069	0.0060
					RMS	0.0048
α_s (205 GeV)	0.0980	0.0978	0.1017	0.1033	0.0976	0.1000
$\pm\Delta$ stat.	0.0053	0.0044	0.0051	0.0047	0.0039	0.0041
$\pm\Delta$ sys. exp.	0.0030	0.0026	0.0026	0.0033	0.0012	0.0022
$\pm\Delta$ had.	0.0006	0.0012	0.0028	0.0005	0.0012	0.0008
$\pm\Delta$ μ_R scale	0.0028	0.0031	0.0028	0.0013	0.0048	0.0023
$\pm\Delta_{\mathrm{tot}}$	0.0067	0.0061	0.0070	0.0059	0.0064	0.0052
					RMS	0.0026
α_s (207 GeV)	0.1057	0.1031	0.1090	0.1040	0.1032	0.1033
$\pm\Delta$ stat.	0.0035	0.0032	0.0036	0.0035	0.0028	0.0030
$\pm\Delta$ sys. exp.	0.0031	0.0026	0.0027	0.0034	0.0013	0.0023
$\pm\Delta$ had.	0.0010	0.0010	0.0027	0.0002	0.0006	0.0004
$\pm\Delta$ μ_R scale	0.0028	0.0031	0.0028	0.0013	0.0048	0.0022
$\pm\Delta_{\mathrm{tot}}$	0.0056	0.0052	0.0060	0.0051	0.0057	0.0044
					RMS	0.0025

Table 13. Results of α_s measurements from distributions in NLLA. The data of [10] have been reanalyzed for this analysis

observable	α_s in NLLA					
	1-T	C	$M_{\mathrm{h}}^2/E_{\mathrm{vis}}^2$	B_{max}	B_{sum}	average
fit range	0.09–0.21	0.16–0.28	0.05–0.17	0.07–0.20	0.115–0.24	
α_s (89.5 GeV)	0.1158	0.1034	0.1190	0.1062	0.1080	0.1088
$\pm\Delta$ stat.	0.0006	0.0003	0.0007	0.0009	0.0002	0.0003
$\pm\Delta$ sys. exp.	0.0014	0.0023	0.0041	0.0042	0.0033	0.0018
$\pm\Delta$ had.	0.0042	0.0032	0.0062	0.0031	0.0042	0.0032
$\pm\Delta$ X scale	0.0059	0.0054	0.0063	0.0067	0.0067	0.0054
$\pm\Delta_{\mathrm{tot}}$	0.0074	0.0067	0.0097	0.0085	0.0086	0.0066
					RMS	0.0066
α_s (91.2 GeV)	0.1167	0.1034	0.1197	0.10056	0.1075	0.1081
$\pm\Delta$ stat.	0.0003	0.0002	0.0003	0.0003	0.0002	0.0002
$\pm\Delta$ sys. exp.	0.0014	0.0023	0.0041	0.0042	0.0033	0.0018
$\pm\Delta$ had.	0.0042	0.0032	0.0062	0.0031	0.0042	0.0032
$\pm\Delta$ X scale	0.0059	0.0054	0.0063	0.0067	0.0067	0.0054
$\pm\Delta_{\mathrm{tot}}$	0.0074	0.0067	0.0097	0.0085	0.0086	0.0066
					RMS	0.0083
α_s (93.0 GeV)	0.1141	0.1013	0.1176	0.1038	0.1062	0.1080
$\pm\Delta$ stat.	0.0005	0.0003	0.0006	0.0009	0.0002	0.0003
$\pm\Delta$ sys. exp.	0.0014	0.0023	0.0041	0.0042	0.0033	0.0018
$\pm\Delta$ had.	0.0042	0.0032	0.0062	0.0031	0.0042	0.0032
$\pm\Delta$ X scale	0.0059	0.0054	0.0063	0.0067	0.0067	0.0054
$\pm\Delta_{\mathrm{tot}}$	0.0074	0.0067	0.0097	0.0085	0.0086	0.0066
					RMS	0.0070

Table 14. Results of α_s measurements from distributions in NLLA

observable fit range	α_s in NLLA					average
	1-T 0.05–0.09	C 0.16–0.28	$M_{\mathrm{h}}^2/E_{\mathrm{vis}}^2$ 0.03–0.05	B_{max} 0.05–0.07	B_{sum} 0.06–0.115	
α_s (183 GeV)	0.0942	0.0971	0.1088	0.1029	0.1000	0.1000
$\pm\Delta$ stat.	0.0055	0.0052	0.0041	0.0097	0.0055	0.0037
$\pm\Delta$ sys. exp.	0.0022	0.0023	0.0024	0.0026	0.0012	0.0016
$\pm\Delta$ had.	0.0015	0.0023	0.0032	0.0005	0.0016	0.0020
$\pm\Delta$ X scale	0.0044	0.0042	0.0035	0.0037	0.0054	0.0044
$\pm\Delta_{\mathrm{tot}}$	0.0075	0.0074	0.0067	0.0107	0.0079	0.0063
RMS						0.0056
α_s (189 GeV)	0.1052	0.1005	0.1066	0.1026	0.1031	0.1021
$\pm\Delta$ stat.	0.0035	0.0031	0.0038	0.0057	0.0031	0.0026
$\pm\Delta$ sys. exp.	0.0024	0.0023	0.0024	0.0028	0.0012	0.0015
$\pm\Delta$ had.	0.0025	0.0025	0.0031	0.0005	0.0019	0.0021
$\pm\Delta$ X scale	0.0044	0.0041	0.0035	0.0037	0.0053	0.0041
$\pm\Delta_{\mathrm{tot}}$	0.0066	0.0062	0.0065	0.0074	0.0065	0.0055
RMS						0.0024
α_s (192 GeV)	0.1058	0.0906	0.1007	0.0890	0.0998	0.0998
$\pm\Delta$ stat.	0.0101	0.0090	0.0110	0.0099	0.0082	0.0071
$\pm\Delta$ sys. exp.	0.0026	0.0024	0.0025	0.0029	0.0012	0.0016
$\pm\Delta$ had.	0.0028	0.0017	0.0033	0.0007	0.0019	0.0019
$\pm\Delta$ X scale	0.0043	0.0041	0.0035	0.0037	0.0053	0.0044
$\pm\Delta_{\mathrm{tot}}$	0.0116	0.0103	0.0123	0.0110	0.0100	0.0087
RMS						0.0071
α_s (196 GeV)	0.1007	0.0945	0.0974	0.1013	0.0962	0.0960
$\pm\Delta$ stat.	0.0057	0.0050	0.0060	0.0090	0.0047	0.0038
$\pm\Delta$ sys. exp.	0.0027	0.0024	0.0025	0.0030	0.0012	0.0015
$\pm\Delta$ had.	0.0015	0.0024	0.0017	0.0008	0.0017	0.0019
$\pm\Delta$ X scale	0.0043	0.0041	0.0034	0.0036	0.0052	0.0042
$\pm\Delta_{\mathrm{tot}}$	0.0078	0.0073	0.0075	0.0101	0.0073	0.0062
RMS						0.0029

Table 15. Results of α_s measurements from distributions in NLLA

observable fit range	α_s in NLLA					average
	1-T 0.05–0.09	C 0.16–0.28	$M_{\mathrm{h}}^2/E_{\mathrm{vis}}^2$ 0.03–0.05	B_{max} 0.05–0.07	B_{sum} 0.06–0.115	
α_s (200 GeV)	0.0981	0.0864	0.0974	0.1012	0.0953	0.0914
$\pm\Delta$ stat.	0.0058	0.0047	0.0057	0.0085	0.0045	0.0038
$\pm\Delta$ sys. exp.	0.0028	0.0025	0.0026	0.0031	0.0014	0.0017
$\pm\Delta$ had.	0.0024	0.0020	0.0028	0.0006	0.0020	0.0023
$\pm\Delta$ X scale	0.0043	0.0040	0.0034	0.0036	0.0052	0.0041
$\pm\Delta_{\mathrm{tot}}$	0.0081	0.0070	0.0077	0.0098	0.0073	0.0063
RMS						0.0056
α_s (202 GeV)	0.1165	0.1026	0.1005	0.1013	0.1039	0.1072
$\pm\Delta$ stat.	0.0076	0.0071	0.0088	0.0146	0.0072	0.0055
$\pm\Delta$ sys. exp.	0.0028	0.0025	0.0026	0.0031	0.0013	0.0016
$\pm\Delta$ had.	0.0016	0.0017	0.0026	0.0005	0.0020	0.0021
$\pm\Delta$ X scale	0.0043	0.0040	0.0034	0.0036	0.0052	0.0041
$\pm\Delta_{\mathrm{tot}}$	0.0093	0.0087	0.0101	0.0154	0.0092	0.0073
RMS						0.0066
α_s (205 GeV)	0.0928	0.0970	0.1032	0.1039	0.1036	0.0996
$\pm\Delta$ stat.	0.0056	0.0050	0.0062	0.0098	0.0049	0.0039
$\pm\Delta$ sys. exp.	0.0030	0.0026	0.0026	0.0031	0.0013	0.0015
$\pm\Delta$ had.	0.0029	0.0023	0.0024	0.0005	0.0017	0.0022
$\pm\Delta$ X scale	0.0042	0.0040	0.0034	0.0036	0.0051	0.0041
$\pm\Delta_{\mathrm{tot}}$	0.0081	0.0073	0.0079	0.0109	0.0074	0.0063
RMS						0.0050
α_s (207 GeV)	0.1054	0.0935	0.1012	0.0972	0.0975	0.0976
$\pm\Delta$ stat.	0.0043	0.0038	0.0047	0.0066	0.0036	0.0030
$\pm\Delta$ sys. exp.	0.0031	0.0026	0.0027	0.0034	0.0013	0.0016
$\pm\Delta$ had.	0.0019	0.0018	0.0025	0.0005	0.0016	0.0019
$\pm\Delta$ X scale	0.0042	0.0040	0.0034	0.0036	0.0051	0.0040
$\pm\Delta_{\mathrm{tot}}$	0.0070	0.0064	0.0069	0.0083	0.0066	0.0056
RMS						0.0045

Table 16. Results of α_s measurements from distributions in $\mathcal{O}(\alpha_s^2)$+NLLA. The data of [10] have been reanalyzed for this analysis

observable	α_s in $\mathcal{O}(\alpha_s^2)$+NLLA (logR)					average
	1-T	C	M_h^2/E_{vis}^2	B_{max}	B_{sum}	
fit range	0.09–0.21	0.16–0.6	0.05–0.17	0.07–0.20	0.115–0.24	
α_s(89.5 GeV)	0.1257	0.1211	0.1226	0.1155	0.1249	0.1220
$\pm\Delta$ stat.	0.0002	0.0002	0.0004	0.0004	0.0001	0.0004
$\pm\Delta$ sys. exp.	0.0021	0.0022	0.0023	0.0021	0.0019	0.0020
$\pm\Delta$ had.	0.0031	0.0021	0.0019	0.0023	0.0029	0.0020
$\pm\Delta$ X scale	0.0060	0.0057	0.0048	0.0051	0.0073	0.0048
$\pm\Delta_{tot}$	0.0071	0.0065	0.0057	0.0060	0.0081	0.0056
					RMS	0.0040
α_s(91.2 GeV)	0.1256	0.1211	0.1230	0.1156	0.1250	0.1219
$\pm\Delta$ stat.	0.0002	0.0002	0.0002	0.0001	0.0001	0.0002
$\pm\Delta$ sys. exp.	0.0021	0.0022	0.0023	0.0021	0.0019	0.0020
$\pm\Delta$ had.	0.0031	0.0021	0.0019	0.0023	0.0029	0.0020
$\pm\Delta$ X scale	0.0060	0.0057	0.0048	0.0051	0.0073	0.0048
$\pm\Delta_{tot}$	0.0071	0.0065	0.0057	0.0060	0.0081	0.0056
					RMS	0.0040
α_s(93.0 GeV)	0.1257	0.1211	0.1208	0.1144	0.1235	0.1222
$\pm\Delta$ stat.	0.0002	0.0002	0.0004	0.0004	0.0001	0.0004
$\pm\Delta$ sys. exp.	0.0021	0.0022	0.0023	0.0021	0.0019	0.0020
$\pm\Delta$ had.	0.0031	0.0021	0.0019	0.0023	0.0029	0.0020
$\pm\Delta$ X scale	0.0060	0.0057	0.0048	0.0051	0.0073	0.0048
$\pm\Delta_{tot}$	0.0071	0.0065	0.0057	0.0060	0.0081	0.0056
					RMS	0.0042

Table 17. Results of α_s measurements from distributions in $\mathcal{O}(\alpha_s^2)$+NLLA

observable	α_s in $\mathcal{O}(\alpha_s^2)$+NLLA (logR)					average
	1-T	C	M_h^2/E_{vis}^2	B_{max}	B_{sum}	
fit range	0.05–0.21	0.16–0.6	0.03–0.17	0.05–0.20	0.06–0.24	
α_s(183 GeV)	0.1072	0.1111	0.1094	0.1049	0.1119	0.1081
$\pm\Delta$ stat.	0.0043	0.0036	0.0037	0.0037	0.0039	0.0034
$\pm\Delta$ sys. exp.	0.0022	0.0023	0.0024	0.0026	0.0012	0.0021
$\pm\Delta$ had.	0.0017	0.0017	0.0031	0.0005	0.0016	0.0011
$\pm\Delta$ X scale	0.0044	0.0042	0.0035	0.0037	0.0054	0.0037
$\pm\Delta_{tot}$	0.0068	0.0062	0.0064	0.0059	0.0070	0.0056
					RMS	0.0029
α_s(189 GeV)	0.1105	0.1101	0.1079	0.1032	0.1122	0.1067
$\pm\Delta$ stat.	0.0027	0.0023	0.0027	0.0024	0.0021	0.0022
$\pm\Delta$ sys. exp.	0.0024	0.0023	0.0024	0.0028	0.0012	0.0020
$\pm\Delta$ had.	0.0020	0.0020	0.0031	0.0005	0.0016	0.0010
$\pm\Delta$ X scale	0.0044	0.0041	0.0035	0.0037	0.0053	0.0038
$\pm\Delta_{tot}$	0.0060	0.0056	0.0059	0.0052	0.0060	0.0049
					RMS	0.0035
α_s(192 GeV)	0.1124	0.1083	0.1082	0.1051	0.1139	0.1096
$\pm\Delta$ stat.	0.0068	0.0060	0.0063	0.0060	0.0052	0.0051
$\pm\Delta$ sys. exp.	0.0026	0.0024	0.0025	0.0029	0.0012	0.0018
$\pm\Delta$ had.	0.0017	0.0014	0.0032	0.0007	0.0019	0.0015
$\pm\Delta$ X scale	0.0043	0.0041	0.0035	0.0037	0.0053	0.0040
$\pm\Delta_{tot}$	0.0086	0.0078	0.0083	0.0077	0.0078	0.0069
					RMS	0.0035
α_s(196 GeV)	0.1045	0.1079	0.1060	0.1024	0.1107	0.1068
$\pm\Delta$ stat.	0.0042	0.0038	0.0040	0.0038	0.0032	0.0033
$\pm\Delta$ sys. exp.	0.0027	0.0024	0.0025	0.0030	0.0012	0.0019
$\pm\Delta$ had.	0.0013	0.0013	0.0029	0.0008	0.0017	0.0014
$\pm\Delta$ X scale	0.0043	0.0041	0.0034	0.0036	0.0052	0.0038
$\pm\Delta_{tot}$	0.0067	0.0062	0.0065	0.0061	0.0065	0.0055
					RMS	0.0036

Table 18. Results of α_s measurements from distributions in $\mathcal{O}(\alpha_s^2)$+NLLA

observable	1-T	C	M_h^2/E_{vis}^2	B_{max}	B_{sum}	average
		α_s in $\mathcal{O}(\alpha_s^2)$+NLLA (logR)	
fit range	0.05–0.21	0.16–0.6	0.03–0.17	0.05–0.20	0.06–0.24	
$\alpha_s(200\,\mathrm{GeV})$	0.1095	0.1044	0.1045	0.1021	0.1101	0.1044
$\pm\Delta$ stat.	0.0041	0.0036	0.0034	0.0036	0.0032	0.0031
$\pm\Delta$ sys. exp.	0.0028	0.0025	0.0026	0.0031	0.0012	0.0020
$\pm\Delta$ had.	0.0023	0.0022	0.0030	0.0006	0.0020	0.0015
$\pm\Delta$ X scale	0.0043	0.0040	0.0034	0.0036	0.0052	0.0037
$\pm\Delta_{tot}$	0.0071	0.0063	0.0062	0.0060	0.0066	0.0054
					RMS	0.0036
$\alpha_s(202\,\mathrm{GeV})$	0.1188	0.1160	0.1105	0.1103	0.1194	0.1141
$\pm\Delta$ stat.	0.0058	0.0050	0.0055	0.0053	0.0047	0.0046
$\pm\Delta$ sys. exp.	0.0028	0.0025	0.0026	0.0031	0.0012	0.0019
$\pm\Delta$ had.	0.0018	0.0015	0.0031	0.0005	0.0016	0.0014
$\pm\Delta$ X scale	0.0043	0.0040	0.0034	0.0036	0.0052	0.0038
$\pm\Delta_{tot}$	0.0081	0.0070	0.0074	0.0071	0.0074	0.0064
					RMS	0.0044
$\alpha_s(205\,\mathrm{GeV})$	0.1023	0.1064	0.1041	0.1031	0.1109	0.1071
$\pm\Delta$ stat.	0.0045	0.0037	0.0041	0.0038	0.0033	0.0033
$\pm\Delta$ sys. exp.	0.0030	0.0026	0.0026	0.0033	0.0012	0.0019
$\pm\Delta$ had.	0.0021	0.0017	0.0027	0.0005	0.0017	0.0012
$\pm\Delta$ X scale	0.0042	0.0040	0.0034	0.0036	0.0051	0.0037
$\pm\Delta_{tot}$	0.0072	0.0063	0.0065	0.0061	0.0064	0.0055
					RMS	0.0035
$\alpha_s(207\,\mathrm{GeV})$	0.1118	0.1074	0.1058	0.1021	0.1134	0.1061
$\pm\Delta$ stat.	0.0036	0.0026	0.0031	0.0029	0.0025	0.0026
$\pm\Delta$ sys. exp.	0.0031	0.0026	0.0027	0.0034	0.0013	0.0020
$\pm\Delta$ had.	0.0016	0.0014	0.0027	0.0005	0.0016	0.0012
$\pm\Delta$ X scale	0.0042	0.0040	0.0034	0.0036	0.0051	0.0037
$\pm\Delta_{tot}$	0.0064	0.0056	0.0060	0.0058	0.0060	0.0051
					RMS	0.0050

Table 19. Results of α_s measurements from mean values with power corrections. The data of [10] and [33] have been reanalyzed for this analysis

Observable	$\langle 1-T\rangle$	$\langle C\rangle$	$\langle M_h^2/E_{vis}^2\rangle$	$\langle B_{max}\rangle$	$\langle B_{sum}\rangle$	average
	α_s from mean values with power corrections		
$\alpha_s(45\,\mathrm{GeV})$	0.1341	0.1418	0.1268	0.1358	0.1421	0.1370
$\pm\Delta$ stat.	0.0154	0.0165	0.0140	0.0127	0.0091	0.0043
$\pm\Delta$ sys. exp.	0.0036	0.0037	0.0026	0.0005	0.0005	0.0023
$\pm\Delta$ μ_R scale	0.0072	0.0055	0.0041	0.0062	0.0052	0.0051
$\pm\Delta$ μ_I scale	0.0052	0.0038	0.0035	0.0005	0.0001	0.0016
$\pm\Delta_{tot}$	0.0181	0.0181	0.0152	0.0142	0.0105	0.0073
					RMS	0.0063
$\alpha_s(66\,\mathrm{GeV})$	0.1159	0.1252	0.1140	0.1189	0.1265	0.1251
$\pm\Delta$ stat.	0.0080	0.0081	0.0076	0.0070	0.0055	0.0043
$\pm\Delta$ sys. exp.	0.0023	0.0028	0.0032	0.0009	0.0006	0.0010
$\pm\Delta$ μ_R scale	0.0059	0.0045	0.0034	0.0051	0.0043	0.0041
$\pm\Delta$ μ_I scale	0.0054	0.0049	0.0030	0.0012	0.0009	0.0019
$\pm\Delta_{tot}$	0.0116	0.0109	0.0094	0.0088	0.0070	0.0064
					RMS	0.0055
$\alpha_s(76\,\mathrm{GeV})$	0.1302	0.1388	0.1235	0.1244	0.1313	0.1255
$\pm\Delta$ stat.	0.0074	0.0077	0.0072	0.0070	0.0053	0.0039
$\pm\Delta$ sys. exp.	0.0032	0.0040	0.0034	0.0020	0.0016	0.0023
$\pm\Delta$ μ_R scale	0.0055	0.0042	0.0032	0.0048	0.0040	0.0038
$\pm\Delta$ μ_I scale	0.0024	0.0013	0.0018	0.0006	0.0004	0.0008
$\pm\Delta_{tot}$	0.0101	0.0098	0.0087	0.0088	0.0068	0.0060
					RMS	0.0062
$\alpha_s(89\,\mathrm{GeV})$	0.1189	0.1263	0.1152	0.1163	0.1235	0.1177
$\pm\Delta$ stat.	0.0004	0.0004	0.0004	0.0003	0.0002	0.0003
$\pm\Delta$ sys. exp.	0.0015	0.0013	0.0019	0.0003	0.0004	0.0009
$\pm\Delta$ μ_R scale	0.0052	0.0039	0.0029	0.0044	0.0037	0.0031
$\pm\Delta$ μ_I scale	0.0031	0.0027	0.0019	0.0009	0.0007	0.0010
$\pm\Delta_{tot}$	0.0063	0.0050	0.0040	0.0046	0.0038	0.0034
					RMS	0.0048
$\alpha_s(91.2\,\mathrm{GeV})$	0.1193	0.1270	0.1153	0.1167	0.1238	0.1176
$\pm\Delta$ stat.	0.0002	0.0001	0.0001	0.0001	0.0001	0.0001
$\pm\Delta$ sys. exp.	0.0015	0.0013	0.0019	0.0008	0.0007	0.0011
$\pm\Delta$ μ_R scale	0.0051	0.0039	0.0029	0.0044	0.0037	0.0031
$\pm\Delta$ μ_I scale	0.0030	0.0025	0.0019	0.0008	0.0007	0.0010
$\pm\Delta_{tot}$	0.0061	0.0048	0.0039	0.0046	0.0038	0.0034
					RMS	0.0049

Table 20. Results of α_s measurements from mean values with power corrections. The data of [10] have been reanalyzed for this analysis

Observable	α_s from mean values with power corrections					
	$\langle 1\text{-}T\rangle$	$\langle C\rangle$	$\langle M_h^2/E_{\text{vis}}^2\rangle$	$\langle B_{\max}\rangle$	$\langle B_{\text{sum}}\rangle$	average
α_s(93 GeV)	0.1182	0.1255	0.1145	0.1157	0.1226	0.1171
$\pm\Delta$ stat.	0.0004	0.0003	0.0004	0.0003	0.0002	0.0003
$\pm\Delta$ sys. exp.	0.0013	0.0011	0.0017	0.0006	0.0004	0.0009
$\pm\Delta$ μ_R scale	0.0051	0.0039	0.0029	0.0044	0.0037	0.0031
$\pm\Delta$ μ_I scale	0.0030	0.0026	0.0019	0.0009	0.0007	0.0010
$\pm\Delta_{\text{tot}}$	0.0061	0.0048	0.0039	0.0045	0.0038	0.0033
					RMS	0.0047
α_s(133 GeV)	0.1158	0.1203	0.1120	0.1109	0.1163	0.1150
$\pm\Delta$ stat.	0.0047	0.0039	0.0048	0.0038	0.0026	0.0023
$\pm\Delta$ sys. exp.	0.0010	0.0011	0.0009	0.0016	0.0011	0.0011
$\pm\Delta$ μ_R scale	0.0043	0.0033	0.0025	0.0037	0.0031	0.0030
$\pm\Delta$ μ_I scale	0.0020	0.0019	0.0013	0.0007	0.0006	0.0010
$\pm\Delta_{\text{tot}}$	0.0067	0.0056	0.0056	0.0056	0.0043	0.0041
					RMS	0.0037
α_s(161 GeV)	0.1037	0.1131	0.1020	0.1053	0.1083	0.1068
$\pm\Delta$ stat.	0.0069	0.0067	0.0068	0.0053	0.0038	0.0031
$\pm\Delta$ sys. exp.	0.0052	0.0066	0.0060	0.0038	0.0023	0.0026
$\pm\Delta$ μ_R scale	0.0040	0.0031	0.0023	0.0034	0.0029	0.0028
$\pm\Delta$ μ_I scale	0.0023	0.0020	0.0014	0.0007	0.0008	0.0010
$\pm\Delta_{\text{tot}}$	0.0098	0.0101	0.0094	0.0074	0.0053	0.0050
					RMS	0.0044
α_s(172 GeV)	0.1140	0.1164	0.1107	0.1119	0.1167	0.1130
$\pm\Delta$ stat.	0.0112	0.0090	0.0106	0.0080	0.0069	0.0061
$\pm\Delta$ sys. exp.	0.0021	0.0036	0.0011	0.0020	0.0048	0.0031
$\pm\Delta$ μ_R scale	0.0039	0.0030	0.0022	0.0034	0.0028	0.0031
$\pm\Delta$ μ_I scale	0.0015	0.0016	0.0010	0.0004	0.0004	0.0011
$\pm\Delta_{\text{tot}}$	0.0121	0.0103	0.0109	0.0089	0.0089	0.0076
					RMS	0.0027

Table 21. Results of α_s measurements from mean values with power corrections

observable	α_s from mean values with power corrections					
	$\langle 1\text{-}T\rangle$	$\langle C\rangle$	$\langle M_h^2/E_{\text{vis}}^2\rangle$	$\langle B_{\max}\rangle$	$\langle B_{\text{sum}}\rangle$	average
α_s(183 GeV)	0.1156	0.1172	0.1067	0.1059	0.1121	0.1121
$\pm\Delta$ stat.	0.0047	0.0038	0.0058	0.0042	0.0026	0.0022
$\pm\Delta$ sys. exp.	0.0045	0.0061	0.0032	0.0044	0.0011	0.0013
$\pm\Delta$ μ_R scale	0.0038	0.0029	0.0022	0.0033	0.0027	0.0029
$\pm\Delta$ μ_I scale	0.0013	0.0014	0.0010	0.0005	0.0005	0.0005
$\pm\Delta_{\text{tot}}$	0.0077	0.0079	0.0071	0.0069	0.0040	0.0039
					RMS	0.0051
α_s(189 GeV)	0.1092	0.1185	0.1022	0.1039	0.1085	0.1082
$\pm\Delta$ stat.	0.0032	0.0024	0.0040	0.0028	0.0017	0.0017
$\pm\Delta$ sys. exp.	0.0044	0.0061	0.0032	0.0044	0.0011	0.0012
$\pm\Delta$ μ_R scale	0.0037	0.0029	0.0021	0.0032	0.0027	0.0027
$\pm\Delta$ μ_I scale	0.0016	0.0013	0.0011	0.0006	0.0006	0.0006
$\pm\Delta_{\text{tot}}$	0.0068	0.0073	0.0057	0.0061	0.0035	0.0034
					RMS	0.0064
α_s(192 GeV)	0.0984	0.1056	0.0947	0.0980	0.1055	0.1092
$\pm\Delta$ stat.	0.0093	0.0066	0.0127	0.0074	0.0045	0.0028
$\pm\Delta$ sys. exp.	0.0040	0.0057	0.0030	0.0042	0.0010	0.0015
$\pm\Delta$ μ_R scale	0.0037	0.0028	0.0021	0.0032	0.0027	0.0030
$\pm\Delta$ μ_I scale	0.0021	0.0021	0.0013	0.0007	0.0007	0.0009
$\pm\Delta_{\text{tot}}$	0.0110	0.0094	0.0133	0.0091	0.0054	0.0044
					RMS	0.0049
α_s(196 GeV)	0.1165	0.1124	0.1036	0.1072	0.1100	0.1092
$\pm\Delta$ stat.	0.0057	0.0044	0.0070	0.0048	0.0030	0.0023
$\pm\Delta$ sys. exp.	0.0045	0.0059	0.0032	0.0044	0.0011	0.0014
$\pm\Delta$ μ_R scale	0.0037	0.0028	0.0021	0.0032	0.0027	0.0029
$\pm\Delta$ μ_I scale	0.0012	0.0016	0.0010	0.0005	0.0005	0.0006
$\pm\Delta_{\text{tot}}$	0.0082	0.0080	0.0081	0.0072	0.0042	0.0039
					RMS	0.0049

Table 22. Results of α_s measurements from mean values with power corrections

observable	$\langle 1\text{-T}\rangle$	$\langle C\rangle$	$\langle M_{\mathrm{h}}^2/E_{\mathrm{vis}}^2\rangle$	$\langle B_{\max}\rangle$	$\langle B_{\mathrm{sum}}\rangle$	average
			α_s from mean values with power corrections			
$\alpha_s(200\,\mathrm{GeV})$	0.1068	0.1104	0.1062	0.1056	0.1096	0.1105
$\pm\Delta$ stat.	0.0057	0.0043	0.0069	0.0048	0.0030	0.0023
$\pm\Delta$ sys. exp.	0.0042	0.0058	0.0032	0.0044	0.0011	0.0014
$\pm\Delta\ \mu_R$ scale	0.0037	0.0028	0.0021	0.0032	0.0026	0.0028
$\pm\Delta\ \mu_I$ scale	0.0016	0.0017	0.0009	0.0005	0.0005	0.0006
$\pm\Delta_{\mathrm{tot}}$	0.0082	0.0079	0.0079	0.0072	0.0042	0.0039
					RMS	0.0022
$\alpha_s(202\,\mathrm{GeV})$	0.0946	0.1066	0.1085	0.1070	0.1127	0.1185
$\pm\Delta$ stat.	0.0097	0.0063	0.0101	0.0067	0.0040	0.0023
$\pm\Delta$ sys. exp.	0.0040	0.0057	0.0032	0.0044	0.0011	0.0015
$\pm\Delta\ \mu_R$ scale	0.0036	0.0028	0.0021	0.0031	0.0026	0.0029
$\pm\Delta\ \mu_I$ scale	0.0022	0.0019	0.0009	0.0005	0.0004	0.0008
$\pm\Delta_{\mathrm{tot}}$	0.0114	0.0091	0.0108	0.0086	0.0049	0.0041
					RMS	0.0068
$\alpha_s(205\,\mathrm{GeV})$	0.0877	0.0879	0.0942	0.0991	0.1003	0.1042
$\pm\Delta$ stat.	0.0072	0.0054	0.0078	0.0050	0.0033	0.0023
$\pm\Delta$ sys. exp.	0.0037	0.0052	0.0030	0.0042	0.0011	0.0013
$\pm\Delta\ \mu_R$ scale	0.0036	0.0028	0.0021	0.0031	0.0026	0.0028
$\pm\Delta\ \mu_I$ scale	0.0025	0.0030	0.0012	0.0006	0.0008	0.0010
$\pm\Delta_{\mathrm{tot}}$	0.0092	0.0085	0.0087	0.0072	0.0044	0.0040
					RMS	0.0060
$\alpha_s(207\,\mathrm{GeV})$	0.1063	0.1077	0.1049	0.1055	0.1070	0.1072
$\pm\Delta$ stat.	0.0047	0.0036	0.0055	0.0040	0.0024	0.0020
$\pm\Delta$ sys. exp.	0.0042	0.0057	0.0032	0.0044	0.0010	0.0012
$\pm\Delta\ \mu_R$ scale	0.0036	0.0028	0.0020	0.0031	0.0026	0.0027
$\pm\Delta\ \mu_I$ scale	0.0015	0.0018	0.0009	0.0005	0.0006	0.0006
$\pm\Delta_{\mathrm{tot}}$	0.0074	0.0075	0.0068	0.0067	0.0037	0.0036
					RMS	0.0011

distributions are compared to predictions in $\mathcal{O}(\alpha_s^2)$, pure NLLA and $\mathcal{O}(\alpha_s^2)$+NLLA (logR), folded with fragmentation models, while from the mean values, α_s is extracted using an analytical power correction ansatz. The α_s values are combined with results obtained at other LEP2 energies and at and around M_Z. This allows both a combined measurement of α_s and a test of the running of α_s. In these combinations the full correlation between energies and observables was taken into account.

The main aim of this study is the comparison of different methods to extract α_s and its scale dependence. Within their uncertainties all techniques yield consistent results. The α_s with smallest uncertainty is obtained from $\mathcal{O}(\alpha_s^2)$ with experimentally optimised scales:

$$\alpha_s(M_Z) = 0.1157 \pm 0.0008\,(\mathrm{stat}) \pm 0.0016\,(\mathrm{sys.ex.})$$
$$\pm 0.0016\,(\mathrm{had}) \pm 0.0022\,(\mathrm{scale})$$
$$= 0.1157 \pm 0.0033\,(\mathrm{tot})\,.$$

The current world average from the particle data group is 0.1172 ± 0.0020 [34].

For the energy dependence of the strong coupling the highest precision is obtained for the α_s values derived from mean values with power corrections:

$$\frac{\mathrm{d}\alpha_s^{-1}}{\mathrm{d}\log\sqrt{s}} = 1.11 \pm 0.09\,(\mathrm{stat}) \pm 0.19\,(\mathrm{sys})$$

The last number has to be compared with the QCD expectation of 1.27.

References

1. H. Fritzsch, M. Gell-Mann, H. Leutwyler, Phys. Lett. B **47**, 365 (1973); D.J. Gross, F. Wilczek, Phys. Rev. D **8**, 3633 (1973); Phys. Rev. D **9**, 980 (1974); H.D. Politzer, Phys. Rep. **14**, 129 (1974)
2. D.J. Gross, F. Wilczek, Phys. Rev. Lett. **30**, 1343 (1973); H.D. Politzer, Phys. Rev. Lett **30**, 1346 (1973).
3. T. Sjöstrand, Comput. Phys. Commun. **39**, 347 (1986)
4. L. Lönnblad, Comput. Phys. Commun. **71**, 15 (1992)
5. G. Marchesini et al., Comput. Phys. Commun. **67**, 465 (1992)
6. Y.L. Dokshitzer, B.R. Webber, Phys. Lett. B **352**, 451 (1995)
7. R.K. Ellis, D.A. Ross, A.E. Terrano, Nucl. Phys B **178**, 412 (1981)
8. S. Catani et al., Phys. Lett. B **295**, 269 (1992)
9. S. Catani et al., Nucl. Phys. B **407**, 3 (1993); Yu.L. Dokshitzer et al., J. High Energy Phys. **1**, 11 (1998); S. Catani et al., Phys. Lett. B **427**, 377 (1998)
10. DELPHI Coll., P. Abreu et al., Phys.Lett. B **456**, 322 (1999)
11. DELPHI Coll., P. Abreu et al., Nucl. Instr. Methods A **303**, 233 (1991)
12. DELPHI Coll., P. Abreu et al., Nucl. Instr. Methods A **378**, 57 (1996)
13. P. Abreu et al., Nucl. Instr. Methods A **427**, 487 (1999)
14. E. Accomando, A. Ballestrero Comput. Phys. Commun. **99**, 270 (1997); E. Accomando, A. Ballestrero, E. Maina, Comput. Phys. Commun. **150**, 166 (2003)
15. A. Ballestrero al. Four-fermion simulation at LEP2 in DELPHI, Comput. Phys. Commun. **152**, 175 (2003)
16. S. Jadach et al., Comput. Phys. Commun. **130**, 260 (2000)
17. DELPHI Coll., P. Abreu et al., Z. Phys. C **73**, 11 (1996)
18. DELPHI Coll., P. Abreu et al., E.Phys.J. C **14**, 557 (2000)
19. G. Salam, D. Wicke, J. High Energy Phys. **5**, 61 (2001)
20. S. Catani, G. Turnock, B.R. Webber, L. Trentadue, Phys. Lett. B **263**, 491 (1991)
21. S. Catani, G. Turnock, B.R. Webber, Phys. Lett. B **272**, 368 (1991)
22. OPAL Coll., P.D. Acton et al., Z.Phys. C **59**, 1 (1993); ALEPH Coll., D. Decamp et al., Phys.Let. B **284**, 163 (1992); L3 Coll. O., Adriani et al., Phys.Let. B **284**, 471 (1992)
23. E. Gardi, J. Rathsman, Nucl. Phys. B **638**, 243 (2002)
24. R. Jones et al., Theoretical uncertainties of α_s from event-shape variables in e^+e^- annihilations, hep-ph/0312016
25. G. Salam et al., Eur. Phys. J. C **24**, 213 (2002)
26. G. Cowan, Statistical Data Analysis, Oxford University Press, 1998
27. B.R. Webber, Hadronic final states, Talk given at workshop on DIS and QCD in Paris, hep-ph/9510283, April 1995
28. Yu.L. Dokshitzer, A. Lucenti, G. Marchesini, G.P. Salam, Nucl. Phys B **511**, 396 (1997)
29. Yu.L. Dokshitzer, A. Lucenti, G. Marchesini, G.P. Salam, JHEP 05(1998) 03
30. Physics at LEP 1, CERN 89-08 Vol. 1 (1989)
31. Yu.L. Dokshitzer et al., Eur. Phys. J. C **3**, 1 (1999)
32. AMY Coll., Y.K. Li et al., Phys. Rev. D **41**, 2675 (1990); CELLO Coll., H.J. Behrend et al., Z. Phys. C **44**, 63 (1989); HRS Coll., D. Bender et al., Phys. Rev. D **31**, 1 (1985); P.A. Movilla Fernandez, et. al. and the JADE Coll., Eur. Phys. J. C **1**, 461 (1998); Mark II Coll., A. Peterson et al., Phys. Rev. D **37**, 1 (1988); PLUTO Coll., C. Berger et al., Z. Phys. C **12**, 297 (1982); TASSO Coll., W. Braunschweig et al., Phys. Lett. B **214**, 293 (1988); TASSO Coll., W. Braunschweig et al., Z. Phys. C **45**, 11 (1989); TASSO Coll., W. Braunschweig et al., Z. Phys. C **47**, 187 (1990); TOPAZ Coll., I. Adachi et al., Phys. Lett. B **227**, 495 (1989); TOPAZ Coll., K. Nagai et al., Phys. Lett. B **278**, 506 (1992); TOPAZ Coll., Y. Ohnishi et al., Phys. Lett. B **313**, 475 (1993)
33. R. Reinhardt WUB-DIS 01-6 and DELPHI Coll., J. Abdallah et al., A study of the energy evolution of event shape distributions and their means with the DELPHI detector at LEP, Eur. Phys. J. C **29**, 285–312 (2003)
34. K. Hagiwara et al., Phys. Rev. D **66**, 010001 (2002)